Basin Research 33.1 (2021): 447-477

DOI: https://doi.org/10.1111/bre.12481

10 Myr evolution of sedimentation rates in a deep marine to non-marine foreland basin system: tectonic and sedimentary controls (Eocene, Tremp-Jaca Basin, Southern Pyrenees, NE Spain)

Running head: Tecto-sedimentary controls on SR evolution

Andreu Vinyoles* (1, 2) - andreu_vinyoles@hotmail.com

Miguel López-Blanco (1, 2) - m.lopezblanco@ub.edu

Miguel Garcés (1, 2) - mgarces@ub.edu

Pau Arbués (1, 2) - pau.arbues@ub.edu

Luis Valero (2, 3) - geo.valero@gmail.com

Elisabet Beamud (2, 3) - betbeamud@ub.edu

Belén Oliva-Urcia (4) - belen.oliva@uam.edu

Patricia Cabello (1, 2) - pcabello@ub.edu

1: Dept. de Dinàmica de la Terra i de l'Oceà, Universitat de Barcelona

2: Geomodels Research Institute, Universitat de Barcelona

3: Paleomagnetic Laboratory CCiTUB-ICTJA CSIC, Barcelona

4: Dept. de Geología y Geoquímica, Universidad Autónoma de Madrid

* Corresponding author

Acknowledgements

We would like to honor Dr. Josep Serra-Kiel for his hard, extensive, and accurate biostratigraphic work on the TJB during most of his scientific career. Without his contribution, an accurate chronostratigraphic framework of the basin would not have been possible to establish. This research was funded by the Spanish project SEROS (CGL2014-55900-P) and by the Generalitat de Catalunya (Grup de Geodinàmica i Anàlisi de Conques - 2017SGR596). AV acknowledges the Ministerio de Economía y Competitividad for

financial support (BES-2015-073302). Thanks to the Laboratory of Paleomagnetism of Barcelona (CCiTUB-ICTJA CSIC). We would like to thank Julian Clark, Maggie Ellis Curry, 2 anonymous reviewers and the editor Nadine McQuarrie for their comments and suggestions that helped to improve the original manuscript. Also we thank the fruitful discussions with Drs. Lluís Cabrera and J.A Muñoz from the Departament de Dinàmica de la Terra i de l'Oceà during the manuscript writing and revision.

ABSTRACT

The propagation of the deformation front in foreland systems is typically accompanied by the incorporation of parts of the basin into wedge-top piggy-back basins, this process is likely producing considerable changes to sedimentation rates (SR). Here we investigate the spatial-temporal evolution of SR for the Tremp-Jaca Basin in the Southern Pyrenees during its evolution from a wedge-top, foreredeep, forebulge configuration to a wedge-top stage. SR were controlled by a series of tectonic structures that influenced subsidence distribution and modified the sediment dispersal patterns. We compare the decompacted SR calculated from 12 magnetostratigraphic sections located throughout the Tremp-Jaca Basin represent the full range of depositional environment and times. While the derived long-term SR range between 9.0 and 84.5 cm/kyr, compiled data at the scale of magnetozones (0.1 to 2.5 Myr) yield SR that range from 3.0 to 170 cm/kyr. From this analysis three main types of depocenter are recognized: a regional depocenter in the foredeep depozone; depocenters related to both regional subsidence and salt tectonics in the wedge-top depozone; and a depocenter related to clastic shelf building showing transgressive and regressive trends with graded and non-graded episodes. From the evolution of SR we distinguish two stages. The Lutetian Stage (from 49.1 to 41.2 Ma) portrays a compartmentalized basin characterized by variable SR in dominantly underfilled accommodation areas. The markedly different advance of the deformation front between the Central and Western Pyrenees resulted in a complex distribution of the foreland depozones during this stage. The Bartonian-Priabonian Stage (41.2 to 36.9 Ma) represents the integration of the whole basin into the wedge-top, showing a generalized reduction of SR in a mostly overfilled relatively uniform basin. The stacking of basement units in the hinterland during the whole period produced unusually high SR in the wedge-top depozone.

KEYWORDS

Decompacted sedimentation rates; magnetostratigraphy; Eocene; Tremp-Graus-Ainsa-Jaca basin; sediment routing system; sedimentation-tectonics; salt tectonics

INTRODUCTION

Foreland systems are regions on Earth where the interplay between tectonic and surface processes is best exemplified (DeCelles, 2012; DeCelles & Giles, 1996; Sinclair, 1997). Mountain building, erosion and sediment transfer are intimately coupled to maintain mass balance during orogenic wedge growth and foreland basin evolution (Sadler & Jerolmack, 2014). The stratigraphic record of foreland basins are thus the result of complex interactions between tectonic uplift and loading, eustatic rise and fall and both tectonic and climate modulated sediment fluxes.

This contribution aims to document the sediment volume supplied across the sediment routing system and link these observations to the evolution of basin accommodation driven by subsidence and sea-level changes. In order to quantify sediment accumulation processes and to understand causal relationships, a precise chronostratigraphic framework is required. High-resolution basin-scale correlations are essential to reconstruct the basin evolution and to have a reliable picture of the paleogeographic scenario over time.

Sedimentation rates (SR) are among easiest parameters to extract from well-dated sedimentary successions. They quantify the preserved thickness of strata or sediments deposited per time unit. Studying them across sediment routing systems provides valuable information on the evolution of accommodation space (controlled by sea-level variations and subsidence) and the magnitude of sediment flux. The more detailed the chronostratigraphic framework, the better our understanding will be of the factors and processes that control the sedimentary infill.

Foreland systems are divided into different tectono-depositional areas (DeCelles & Giles, 1996) that result from a subsidence distribution that parallels the main structures of the fold and thrust belt. In addition, as is common in foreland systems, the sediment flux results from interacting axial and transverse routing paths, leading to a basin fill distribution that varies not only perpendicular to the fold-and-thrust belt axis, but also parallel to it. This results in a variable filling of the foreland basin with underfilled and overfilled accommodation areas in the same structural unit.

In this work we investigate the evolution of SR in across the Tremp-Jaca portion of the South-Pyrenean Foreland basin and analyse the varying controls over accommodation in order to understand the tectonosedimentary evolution of the basin. The South-Pyrenean Foreland basin is a good candidate for this purpose since its stratigraphy and sedimentology have been widely studied, the timing of the different thrust and fold structures has been determined and a rather complete magnetostratigraphic

dataset is available in the literature. More specifically, our research builds on a selection of earlier magnetostratigraphic studies in the Eocene Tremp-Jaca basin (TJB) (Beamud *et al.*, 2003; Bentham, 1992; Garcés *et al.*, 2014; Mochales *et al.*, 2012; Oms *et al.*, 2003; Rodríguez-Pintó *et al.*, 2012a; Rodríguez-Pintó *et al.*, 2012b; among others) by presenting two new magnetostratigraphic sections. The collected dataset allows for a comparison of the SR among different tectonic units and areas of the basin. The selected time interval spans from early Lutetian to early Priabonian (*ca*. 49.1 to 36.9 Ma), a key period in the evolution of the basin, as it includes the transition from underfilled to overfilled stages and the progressive incorporation of the basins into the active thrust sheets (Barnolas & Pujalte 2004, Barnolas *et al.*, 2019; Puigdefàbregas & Souquet 1986; Puigdefàbregas *et al.* 1992). Earlier publications documenting SR in the South-Pyrenean foreland were focused on individual stratigraphic sections (*e.g.*, Beamud *et al.*, 2011; Bentham *et al.*, 1992; Bentham & Burbank, 1996; Michael *et al.*, 2014). These studies did not have the resolution to examine the long-term SR trends (*ca.* 10 Myr) of the entire foreland basin system, or provide the temporal detail (100s to 1000s of kyrs) of tectonically-controlled depozones and their relation to the migration of the underfilled to overfilled accommodation boundary (Catuneanu, 2017), as we do in this work.

Sedimentation rates in foreland basins

Foreland basin systems can be divided in different tectono-depositional areas (DeCelles & Giles, 1996) depending on their location relative to the main deformation front. These are: 1) the wedge-top depozone, or the thrust-top and piggy-back basins on top of the orogenic wedge; 2) the foredeep depozone, in between the orogenic wedge and the proximal flank of the forebulge; 3) the forebulge depozone, between the foredeep and back-bulge; and 4) the back-bulge, cratonward of the forebulge (Figure 1).

Many foreland basins develop piggy-back basin sequences, carried by thrust and faults, as a product of forward (*i.e.*, towards the foreland) thrust propagation. This results in a migration of the depocenters and depozones towards the foreland (Figure 1). When the primary foredeep depozone is incorporated into the wedge-top depozone, it becomes a zone of sediment bypass, and eventually may become the source area for the new adjacent foredeep (Bally, 1984; Cant & Stockmal, 1989; DeCelles & Giles, 1996; Miall, 1995). Similarly, the forebulge and backbulge depozones are progressively incorporated into the foredeep as the basin migrates towards the foreland increasing accommodation space and the resulting infill of clastic sediments. Accordingly, the expected evolution of SR at a fixed location would be: (1) An initial

progressive increase while the former distal foreland region is incorporated in the foredeep depozone, and (2) a decrease in SR when it is finally incorporated into a thrust-top basin in the wedge-top depozone, finally becoming part of the source area (Figure 1e) (DeCelles & Giles, 1996; Homewood *et al.*, 1986). However, this documented SR trend in foreland basins may be far more complex, depending on the tectonic evolution and structural control of the wedge-top basins and variability in sediment flux. The structural style of the hinterland may influence different uplift and denudation scenarios, which control both the amount of sediment supply, and the load-related regional flexural subsidence (DeCelles & Giles, 1996; Romans *et al.*, 2016). In addition, the emplacement of thrust sheets in the foreland may promote uplift associated with in-sequence thrusts as the former foredeep is incorporated into the wedge-top depozone and drive local accommodation variations alongside the growth of topographic barriers and traps for clastic sediments. Further differences may arise due to the inherited 3D geometry of the foreland basin, and the relative timing of growing structures. Finally, a sediment supply increase may result in a higher sediment load on the basin that will trigger higher subsidence.

Previous works on SR for foreland basin settings give average values of 10 to >100 cm/kyr (Einsele, 2000). However, very high values—such as 238 cm/kyr (Maesano & D'Ambrogi, 2015)—have been calculated for the Pleistocene of the Po basin, similar to the 270 cm/kyr obtained from the numerical models for the Eocene of the Western Alps (Erdos, *et al.*, 2019).

Geological setting

The Tremp-Jaca basin (TJB) is part of the South-Pyrenean foreland which evolved from late Cretaceous to Miocene times in response to flexural subsidence related to the growth of the Pyrenees (Zoetemeijer *et al.*, 1990). Modern TJB configuration was created by the interaction of several thrusts detached at the evaporitic upper Triassic Keuper facies. Three major thrust sheets constitute the South-Pyrenean fold and thrust belt in its central part. From north to south and in order of emplacement they are: the Cotiella-Bóixols, Peña Montañesa-Montsec, and Sierras Exteriores-Serres Marginals thrust sheets (Figure 2), which were emplaced during late Cretaceous, late Paleocene-Ypresian (60.0 to 47.8 Ma) and Lutetian-Oligocene (47.8 to 23.0 Ma) times, respectively. The southward displacement of these thrust sheets was triggered by basement thrusts in the Axial Zone (Beaumont *et al.* 2000, Cámara & Klimowitz, 1985; Seguret, 1972). The distribution of the Keuper evaporitic facies influenced the thrust motion, producing differential displacement which resulted in the Ainsa Oblique Zone (AOZ) (Muñoz *et al.*, 2013). The AOZ is characterized by a set of kilometer scale N-S trending folds and thrusts (*e.g.*, Mediano, Olsón, Boltaña and Añisclo anticlines, Figure 2a and 2b), originally developed perpendicular to the maximum shortening direction during Lutetian and Bartonian. Their present-day oblique orientation is the result of clockwise

vertical-axis rotations (70° to 55°) developed in response to a divergent thrust transport direction because the differential displacement and change in structural style from the central to the western Pyrenees (Muñoz *et al.*, 2013).

The Eocene TJB is an E-W trending ensemble of sub-basins that were bounded by active tectonic structures. The sediments were mostly derived from the inner zone of the axial Pyrenees growing in the north and distributed towards the west into the Atlantic ocean through an axial drainage system parallel to the chain (Garcés *et al.*, 2020, Nijman & Nio, 1975; Puigdefàbregas *et al.*, 1992). During early Eocene times, the sediment routing system was divided into two connected sub-basins (Figure 2); the proximal wedge-top Tremp-Graus basin, on top of the Peña Montañesa-Montsec thrust sheet, and the distal Ainsa-Jaca basin located to the west in the footwall of the Montsec thrust sheet, progressively incorporated on top of the Gavarnie-Sierras Exteriores thrust sheet (Muñoz *et al.*, 2013).

During the early Eocene, the wedge-top depozone of the thrust-top Tremp-Graus basin was connected to the west with a foredeep depozone in the Ainsa-Jaca basin. During the middle and late Eocene, the Ainsa basin progressively became part of the wedge-top depozone due to the forward migration of the thrust fronts. The development of the AOZ from early Lutetian to late Bartonian (47.8 to 37.0 Ma) separated the Ainsa basin to the East from the Jaca-Pamplona basin to the West (Figure 2) incorporating progressively the AOZ into the wedge-top depozone. This deformation temporally isolated the different depocenters and distorted the paleoflow direction (Dreyer *et al*,. 1999, Grasseau, 2016; Labourdette, 2011; Moody *et al.*, 2012; Muñoz *et al.*, 2013; Pickering & Corregidor, 2005).

Stratigraphy

The deposition of the sedimentary units during the middle-late Eocene took place in a broadly regressive setting (Figure 3). Three fluvial Formations and Groups (Capella, Escanilla, and Campodarbe) were fed from the north by the Pobla de Segur, Sis, Gurp, and Santa Orosia alluvial fans. Towards the west, the fluvial units grade laterally into the transitional detrital formations of Perarrúa, Pano, Sobrarbe, Sabiñánigo, Belsué-Atarés and their prodelta equivalents, San Vicente, Larrés, Pamplona, and Arguís formations (Figure 3). Farther west, they grade into deep sea environments exemplified by the turbiditic systems of the San Vicente Formation and the Hecho Group. Concomitantly, shallow carbonate platforms developed at the southern Jaca basin margin, the Guara Formation.

Along the axis of the Tremp-Graus basin, the middle Eocene sedimentation started with the fluvial Capella formation (Garrido-Mejías, 1968) in the east, grading westwards into the deltaic Perarrúa Formation (Nijman & Nio, 1975). These deltaic units were arranged in a westward regressive trend that was shortly interrupted by a transgressive event represented by the shallow marine Pano Formation (Donselaar &

Nio, 1982) and the Grustán Limestone (Garrido-Mejias, 1968). Overlying them, sediments of the fluvial Escanilla Formation (Garrido-Mejias, 1968) renewed the long-term regressive trend.

Westwards, the lowermost units of the Ainsa basin, correspond to the deposition of the Cuisian to Lutetian (53.0 – 41.2 Ma) San Vicente formation (van Lunsen, 1970), a marly succession that ranges from deep marine turbidite systems to prodelta and carbonate slope facies related to the Guara and Grustán formations. Bathymetry data of the San Vicente Formation suggest upper to mid bathyal depths of 400 to 600 m based in agglutinated foraminifera (Pickering & Corregidor, 2005). However, these isolated data are not applicable to the whole formation since water depths could have varied significantly between sites. Overall, the succession in the Ainsa basin depicts a regressive trend from the slope deep-marine San Vicente Formation, to the shallow deltaic Sobrarbe Formation (de Federico, 1981), and the Lutetian to Priabonian (42 – 37.5 Ma) fluvial Escanilla Formation on top.

The Jaca basin forms an E-W trending synclinorium geometry where middle Eocene sediments crop out at both limbs, herein referred to as the Southern and Northern Jaca Basin. Younger (upper Eocene and Oligocene) strata occupy the syncline axis.

The basal units of the Southern Jaca Basin are the carbonate platforms of the Lutetian (47.8 – 41.2 Ma) Guara Formation (Puigdefàbregas, 1975) with estimated paleobathymetry values ranging from 0 to 60 m in the Arguis section (Huyghe *et al.*, 2012). Above these platforms, a deltaic sequence with the prodeltaic Arguís marls Formation (Puigdefàbregas, 1975) and the delta front of the Belsué-Atarés Formation (Millán *et al.*, 1994; Puigdefàbregas, 1975) were deposited. Vertically, these units are overlain by the non-marine Bartonian to Priabonian (39 - 35 Ma) Campodarbe Group (Soler-Sampere & Puigdefàbregas, 1970).

In the Northern Jaca Basin the Lutetian succession (47.8 – 41.2 Ma) starts with the deep marine turbidites of the Hecho Group (Mutti *et al.*, 1972), although the water depth of these sediments remains widely unconstrained. Interpreted as the distal lobe and basin floor equivalents of the Ainsa basin slope deposits (Mutti *et al.*, 1985; Mutti, 1992), bathymetries should be as deep as those proposed for Ainsa (400 to 600 m) and, as stated above, not extrapolatable for the whole Hecho Group vertical succession in the Jaca Basin. The basin progressively evolved into the shallower prodeltaic environments of the Bartonian (40.8 - 40.2 Ma) Larrés marls Formation (Remacha *et al.*, 1987) and the delta front/delta plain environments of the Bartonian (40.2 – 39.9 Ma) Sabiñánigo sandstone Formation (Puigdefàbregas, 1975). A transgressive event occurred at the top of the Sabiñánigo sandstone, returning to deep-sea sedimentation of the Pamplona marls Formation (Mangin, 1959-60), a lateral equivalent of the Arguís marls Formation of the southern Jaca basin. These are overlain by the Bartonian to Priabonian (39.9 – 35.7 Ma) shallow-marine Belsué-Atarés Formation both in the Northern and Southern Jaca Basin. The top of the succession corresponds to the non-marine Santa Orosia fan of the Campodarbe Group (Puigdefàbregas, 1975).

METHODS

The study of the spatial and temporal evolution of SR in the Central TJB is based on the analysis of selected magnetostratigraphic logs. The integration of previous studies with two new key magnetostratigraphic logs provides the necessary robust chronostratigraphic framework along two roughly E-W profiles. These profiles illustrate the Lutetian to Priabonian (47.8 – 36.9 Ma) evolution of the complete sediment routing system from alluvial fans to deep marine environments. The choice of this time span is based on the good magnetostratigraphic control across the whole basin and sub-basins, the presence of distinct time-equivalent depositional environments from alluvial fans to deep-sea fans, and good age control for relevant tectonic structures. The overall setting is most appropriate to investigate the links between SR, depositional environments, and tectonics, which produced an evolving foreland basin system with well-defined wedge-top, foredeep, and distal foreland depozones during the Lutetian and a relatively uniform wedge-top situation at Bartonian and Priabonian.

A review of existing magnetostratigraphic data

After a critical review of the published data, we selected the magnetostratigraphic logs that include the age range from chrons C22 to C16 (Ypresian-Priabonian, 49.7 – 35.7 Ma) and provide sufficient time-resolution to study the variations in SR (Table 1). We applied the following criteria: (1) logs with an average number of samples/magnetozones lower than 8 were considered to have insufficient resolution (Johnson & McGee, 1983) and were then excluded; (2) magnetostratigraphic logs that correlate with the Global Polarity Time Scale (GPTS) that missed significant geomagnetic chrons were excluded; (3) to better capture the 2D geometry along the basin transects, data far-off from selected segments were ignored; (4) where multiple logs were available, the above quality criteria were applied to select the best log for a specific location. The conclusion of this review is that 10 logs matched the selection criteria for our analysis (see location in Figure 2): Lascuarre (LS), Ésera (ES), and Mediano (MD) (Bentham & Burbank, 1996), Isuela (IS) (Rodríguez-Pintó *et al.*, 2012b), Santa Marina (SM) (Rodríguez-Pintó *et al.*, 2012a), Coscollar and Mondot (CM) (Mochales *et al.*, 2012), Río Aragón/Gállego (GA) (Oms *et al.*, 2003), Pobla de Segur (PS) (Beamud *et al.*, 2003), and Belsué (BL) (Garcés *et al.*, 2014).

Cross-correlation between the above selected logs highlights a problem in the magnetostratigraphic interpretation of the Ésera log (Bentham & Burbank, 1996), particularly its correlation with the Ainsa basin logs. Magnetostratigraphic interpretation of the Ésera log attributed the upper normal magnetozone (N5, Bentham, 1992, p.78) to the chron C20n, placing the Grustán limestone Formation (Figure 3) within chron C19r. This is inconsistent with the stratigraphic correlation of the Grustán limestone Formation to the west. Here, the Grustán Limestone was attributed to middle Lutetian 1, chron C20 (45.9 – 47.8 Ma) (Poblet *et al.*, 1998) and is below the Sobrarbe deltaic complex which records from C20r to C18n magnetozones. We propose to interpret the upper normal magnetozone of the Ésera log as either an artifact or a short geomagnetic event that is not yet identified in the GPTS, resulting in a correlation of the Grustán Formation with chron C20r.

New magnetostratigraphic data

In addition to the compilation of previous magnetostratigraphic sections, we present data for two new magnetostratigraphic logs located on both sides of the Boltaña anticline (Figure 2). Similar magnetostratigraphic logs, previously studied by Bentham & Burbank (1996) and Hogan & Burbank (1996) do not satisfy our quality criteria due to their insufficient resolution to provide a robust correlation with the GPTS. East of the Boltaña anticline, within the Ainsa basin, we measured and sampled the Olsón log (OL) (Figure 4, left), whereas the Yebra de Basa log (YB) (Figure 4, right) was sampled west of the Boltaña anticline, within the Jaca Basin. Aiming to obtain a complete magnetic polarity sequence, the average sampling resolution was 3 meters/site in the Olsón log and 7 meters/site in the Yebra de Basa log. We sampled at relatively homogeneous intervals reaching a total of 194 sites along 690 m in the Olsón log, and 233 sites along more than 1,600 m in the Yebra de Basa log. Further details on the paleomagnetic sampling, laboratory procedures and polarity determination can be found in the Electronic Appendix and in figures 1, 2 and 3.

In order to build a local magnetostratigraphy, the Characteristic Remanent Magnetization (ChRM) directions of high and intermediate quality were considered (Figure 5; Electronic Appendix). Results are obtained from a total of 311 samples (Table 2), which represent 72.8% of the total of samples processed in the laboratory. The mean normal and reversed directions from Yebra de Basa give a positive reversal test class C (McFadden & McElhinny, 1990), while results from the Olsón section show a larger scatter, particularly the reversed polarity directions, yielding a negative reversal test. We conclude that the demagnetization procedure was successful in isolating the ChRM in the marl samples from Yebra de Basa. In contrast, the hematite bearing samples from the Olsón section partially retained a north and down-

directed secondary component, possibly a recent viscous overprint, as suggested by the excessively shallow mean inclination of the reversed polarity direction. The resulting mean direction of the Olsón log records a significant clockwise rotation, averaging 30°. This rotation is less than that recorded by the underlying units of the Sobrarbe deltaic complex in the Ainsa basin (Mochales *et al.*, 2012; Muñoz *et al.*, 2013), which shows evidence for the coeval evolution of the Boltaña Anticline with these units. In contrast, the mean direction of the Yebra de Basa log in the Jaca Basin does not yield any vertical-axis rotation. These results highlight the differential rotation experienced by the Ainsa Basin compared to the Jaca Basin, related to the transition of the Ainsa foredeep into a piggy-back basin, on top of the Gavarnie thrust sheet (Muñoz *et al.*, 2013).

We infer a magnetic polarity at the sample level from calculation of the Virtual Geomagnetic Pole (VGP) latitude for each paleomagnetic direction. Positive and negative latitudes have been interpreted as normal and reversed polarity, respectively (Figures 4 and 5). As the Olsón paleomagnetic directions show significant vertical-axis rotation, a -30° correction has been applied, in order to average a northerly declination before the VGP calculation.

Local magnetozones are defined as stratigraphic intervals of either normal or reversed polarity represented by two or more successive sites. Single sites yielding a polarity opposite to its adjacent sites are not considered sufficiently robust, and are indicated by a half width bar in the polarity log (Figure 4). They could either represent true short geomagnetic features or simply artifacts related to a remanence acquisition delay. In either case, they cannot be used for correlation purposes because the reference time scale is not yet fully resolved for very short geomagnetic chrons.

Sediment decompaction

The decompaction of the different logs was calculated following the methods described by Angevine *et al.* (1992). These equations assume that the thickness of a compacted unit depends on the change of porosity during the burial, but the volume of the grains does not change during compaction. The decreasing compaction coefficient rate of the different lithologies is empirically defined from different studies. Here we have used the data from Angevine *et al.* (1992), choosing an exponential relationship for the change in unit porosity. To perform this calculation requires estimates of the maximum burial of the logs, which range from 210 m in the la Pobla de Segur area to more than 3,000 m in the IS log (Table 3). Overburden values were obtained from Beamud *et al.* (2011), Montes (2009), and Rodríguez-Salgado *et al.* (accepted).

RESULTS

Magnetostratigraphy

The local magnetostratigraphic records of the Olsón and the Yebra de Basa logs were correlated to the Geomagnetic Polarity Time Scale (GPTS) (Gradstein *et al.*, 2012) (Figure 6), aided by their position relative to other published magnetostratigraphic logs (Mondot and Río Gállego-Río Aragón). The base of the Olsón log (Figure 4a) overlaps the uppermost part of the Mondot log (Figure 6) (Mochales *et al.*, 2012). So here we propose that the first reversal magnetozone R1 in Olsón is equivalent to the upper part of Chron C18r (the youngest chron at the Mondot log), and the normal magnetozone (N1) corresponds to Chron C18n. R2 correlates with C17r, and the sequence N2-R3-N3 with the lower part of C17n. In the uppermost part of the sequence, a single-site reversed magnetozone might represent that the C17n/C16r boundary has been reached, but more data should be collected from younger levels to confirm it.

The Yebra de Basa log (Figure 4b) can be correlated with the Río Gállego-Río Aragón log (Oms *et al.*, 2003) (Figure 6), which makes the correlation with the GPTS feasible. The lower R1 in Yebra de Basa underlying the Sabiñánigo Sandstone corresponds to the top of R3 in the Río Gállego-Río Aragón log (Oms *et al.*, 2003), and correlates with C18r. Above R1 the magnetostratigraphic sequence is dominated by normal polarities, with a sequence N1-R2-N3 that correlates to the C18n2n, C18n1r, and C18n1n chrons, and an R3-N3 sequence that correlates to the C17r-C17n pair. The correlation of Olson and Yebra de Basa with the GPTS shows that sedimentation from the base of Bartonian to lowermost Priabonian (41.2 – 37.7 Ma) is recorded at both locations.

The stratigraphic correlation of all logs considered in this study (Figure 7) encompasses a range in age from early Lutetian to early Priabonian (49.5 – 36.7 Ma). The N-profile follows the detrital sediment routing from proximal to distal environments (E-W, SE-NW), following the main sedimentary trough and the axis of the clastic routing system (from PS to GA log) and then turns southwards to the IS and BL logs in the Southern Jaca basin (N-S) (Figure 2). The S-profile (Figure 7) is E-W oriented, first following the sedimentary axis (Tremp-Graus / Ainsa) and then crossing the main sedimentary trough to the Southern Jaca basin (Figure 2).

Sedimentation rates in the Tremp-Jaca basin

The average SR of the complete stratigraphic interval yields long-term compacted SR in the TJB that range from 8.93 cm/kyr in the PS log (Tremp-Graus) to 84.54 cm/kyr in the GA+YB composite log (Northern Jaca) both for a 6.5 Myr interval (Table 3). Compacted SR for these logs are 8.27 cm/kyr and 53.25 cm/kyr respectively. All these values reasonably fit the range of 10 to >100 cm/kyr proposed for foreland basins in Einsele (2000).

Shorter term SR were calculated by decompacting sedimentary units from each magnetozone and dividing by their durations. The SR ranged from 3 to 170 cm/kyr, with average values between 30 and 40 cm/kyr (Table 3). The sedimentation rate trend for each log is shown in Figure 8 for both compacted and decompacted thicknesses. Some of these diagrams (*e.g.,* Mediano (MD), Santa Marina (SM)) roughly depict an increasing then decreasing trend that is typical for a foreland basin infill (Figure 1e). Other logs only show increasing (Río Aragón/Gállego (GA), Isuela (IS), Coscollar/Mondot (CM)) or decreasing SR (Olsón (OL), Yebra de Basa (YB), Lascuarre (LS)), because these only represent a portion of the whole succession at the site, so the complete vertical trend is not recorded. To avoid this incomplete view, and assisted by the magnetostratigraphic framework, we assembled two composite correlation panels comprising the whole stratigraphic succession: The N-profile and the S-profile, showing the vertical and horizontal evolution of the SR (Figure 7b). The panels cover four different basin domains or subbasins: Tremp-Graus, Ainsa, Southern Jaca, and Northern Jaca.

In the Tremp-Graus area (Pobla de Segur (PS), Lascuarre (LS), and Ésera (ES) logs) SR can be higher than 29 cm/kyr (but approximately 15 cm/kyr on average). For a proximal-distal profile (Pobla de Segur (PS)-Lascuarre (LS)), we observe a slight increase in SR towards the distal part (Table 3 and Figure 7).

The Ainsa area (Mediano (MD), Olsón (OL), and Coscollar/Mondot (CM) logs) shows a wide range of SR (in time and space) for most of the Lutetian, reaching maximum values of 68 cm/kyr, minimums close 4 cm/kyr, and average values near 45 cm/kyr. During the Bartonian and Priabonian SR are moderate, close to 20 cm/kyr on average. The general vertical trend is of increasing SR during the Lutetian, followed by a progressive decrease during the Bartonian, to minimum SR at the top of the succession.

The Northern Jaca area (Yebra de Basa (YB) and Río Aragón/Gállego (GA) logs) shows very high SR for most of the succession, with an average of 85 cm/kyr and maximum values of up to 170 cm/kyr (C18n.1r, Yebra de Basa (YB) log). The initially high SR (more than 90 cm/kyr) are punctuated by a transient decrease to 53 cm/kyr at the end of Lutetian, later recovering the high values to a maximum (170 cm/kyr) during the middle Bartonian, and followed by a progressive decrease in the Bartonian-Priabonian.

The Southern Jaca area (Isuela (IS), Belsué (BL), and Santa Marina (SM) logs) depicts low to moderate SR (in most cases below 40 cm/kyr). As for Ainsa, they depict an initial increase in SR (from 3 to 50 cm/kyr)

during the Lutetian. During Bartonian values range between 10 and 56 cm/kyr with no clear general trend when considering short magnetozones.

Decompacted SR in Figure 7 were calculated for every single magnetozone identified in the magnetostratigraphic logs. In the following analysis, short magnetozones were combined (Table 3 and Figure 9) in order to lower the errors in SR related to uncertainties in the location of the magnetozone boundaries. The N-profile (Figure 9) shows a progressive increase of SR from proximal (Tremp-Graus) to the distal area (Northern Jaca), where a persistent major depocenter is established. From the Northern Jaca depocenter a southwards decrease in SR is observed (Figure 9). The Northern Jaca depocenter is characterized by the sedimentation of thick deep marine facies, whereas on the Tremp-Graus, Ainsa, and Southern Jaca alluvial, shallow marine and submarine slope facies are dominant. The last stages of evolution (uppermost Bartonian and Priabonian, 38.4 to 37.0 Ma) evidence a uniformization trend of SR in the Ainsa and Jaca basins.

The S-profile shows the development of a depocenter in the Ésera section (Tremp-Graus basin) during the early Lutetian (47.8 – 43.5 Ma) (Figure 9, C21n and C20r). Later (Figure 9, from C20n to C18r), the depocenter migrated to the Ainsa area for most of the Lutetian and the lowermost Bartonian (43.5 - 40.2 Ma). This depocenter reveals abrupt changes in SR across short spatial distances. In the final stage (40.2 – 36.9 Ma) (Figure 9, from C18n to C17n) SR become more uniform in Ainsa and Southern Jaca like those observed in the N-Profile.

Integrating the N- and S-profiles in map view (Figure 10) we observe that the main depocenters (Northern Jaca and Ainsa in Figure 9) are part of the same sedimentary trough. The N-profile lies aligned with the sedimentary trough axis, whereas the S-profile cuts across it (Figures 9 and 10). Thus, since maximum SR (depocenter) are obtained in Northern Jaca, we will refer to the region of maximum SR in the S-Profile as a relative depocenter.

DISCUSSION

Sedimentation rates and depozones

The extensive structural and stratigraphic work carried out in the TJB (Arbués *et al.*, 2011; Beamud, 2013; Garcés *et al.*, 2020; Millán *et al.*, 1994; Muñoz *et al.*, 2013; Poblet *et al.*, 1998; Puigdefàbregas, 1975; Rodriguez-Pintó, *et al.*, 2016; Roigé *et al.*, 2016, among others) has provided the precise ages and locations of the different frontal structures of the southern Pyrenees in the study area. We have used them for the location of the different foreland depozones relative to the migrating deformation front (Figures 9 and 10). Figure 9 marks the location of depozones for successive chron intervals, from C21n to C17n (47.8 to 36.9 Ma). Figure 10 shows a map view of these depozones with their location relative to the deformation front, as well as the tectonic structures active in each time-slice. The progressive advance of the deformation front is documented together with the westwards and southwards migration of the depozones. The present day "Z-shape" map view of the clastic sediment routing system from Tremp-Graus to Jaca during the Lutetian and early Bartonian (Figure 10 b, e) is a consequence of the progressive clockwise vertical-axis rotation of the AOZ from Lutetian to Oligocene (Mochales *et al.*, 2012; Muñoz *et al.*, 2013). This rotation affects the central part of an E-W to ESE-WNW oriented sedimentary trough, as shown in the reconstructions by Muñoz *et al.* (2013) and Garcés *et al.* (2020). This trough should have shown a relatively straight ESE-WNW orientation during early Lutetian similar to the geometry observed in the maps of the uppermost Bartonian and Bartonian-Priabonian (Figures 10 f, g, and h).

In the studied portion of the TJB, the wedge-top depozone is identified in the hanging wall of active thrusts and related folds. However, the distinction between foredeep and forebulge is not straightforward because the transition between the two zones maybe gradual and difficult to establish (DeCelles & Gilles, 1996). As indicated in DeCelles & Gilles (1996), in underfilled submarine foreland basin systems local carbonate platforms may develop in the forebulge depozone (Allen *et al.*, 1991; Dorobek, 1995; Patton & O'Connor, 1988; Wuellner *et al.*, 1986). Thus, the main sedimentological attributes of some of the studied sections cratonward from the main clastic trough (carbonate platform deposits with low SR) can be interpreted as part of a forebulge depozone (DeCelles & Giles, 1996).

During most of the Lutetian the basin was configured into wedge-top (Tremp-Graus and part of Ainsa in the hanging wall), foredeep (Northern Jaca and part of Ainsa in the footwall) and forebulge (Southern Jaca) depozones (Figures 9 and 10). The forebulge depozone is associated with shallow-marine carbonate

deposition (Guara formation) with relatively low SR (3 to 24 cm/kyr), and it is easily recognizable (logs IS and partially SM and CM in Ainsa) from C21n to C19r (47.8 to 42.4 Ma). The proximal foredeep is characterized by the presence of a distinct depocenter in Northern Jaca (log GA) with high SR (53 to 101 cm/kyr) in the Hecho group deep marine succession from C20n to C19n (43.5 to 41.2 Ma) (Figures 9 and 10). This depocenter is located south to the deformation front in the footwall of the Monte Perdido thrust sheet (Muñoz *et al.*, 2013). The Montsec-Peña Montañesa thrust and its related splays (La Fueba thrust system) were the frontal structures of the Pyrenees until late Ypresian (C21r) (Muñoz *et al.* 2013). Afterwards (C21n), the deformation front shifted 10-15 km towards southwest, starting the emplacement of the Gavarnie thrust sheet which incorporated part of the former Montsec-Peña Montañesa related foredeep depozone to the new wedge-top and creating a new depozone boundary marked by the Añisclo and Olson Anticlines (between MD and CM logs).

During C21n there is a relatively constant low (3 to >12 cm/kyr) SR zone with carbonate platform and slope sedimentation occupying Southern Jaca and eastern Ainsa (IS to CM logs), grading eastwards to higher SR in eastern Ainsa and western Tremp–Graus (>30 cm/kyr) where shallow marine and non-marine sedimentation occurs (S-profile, Figure 9). Thus, the western oblique boundary of the wedge-top depozone is in a location where the expected increase in SR towards non-deformed areas (footwall) does not occur. We do observe instead a westwards decrease from 11 cm/kyr at MD (wedge-top) to 4 cm/kyr at CM (forebulge) (Figure 9; C21n). The absent or very narrow (less than 3.5 km wide) foredeep at this position points to an abrupt transition from forebulge to a thrust-top depozone with moderate SR (>30 to >12 cm/kyr). This sharp transition is due to the differential advance of the Gavarnie trust whose oblique front reached (very close to) the forebulge in southern Ainsa Basin whereas in Jaca Basin the deformation front was located further north (Muñoz *et al.*, 2013, Garcés *et al.*, 2020) with a well-developed foredeep to the south. However, these 2D observations are restricted to the available magnetostratigraphic logs which do not cover the northern Ainsa basin. The N-S cross sections in Cámara & Klimowitz (1985) show an important thickening of the Lower and middle Eocene units towards the north in the Ainsa basin, with the MD and CM logs located close to the southern edge. This implies a northward increase in SR of the wedge-top basin potentially connected to the foredeep growing to the northwest in the Jaca basin (Figures 2 and 10b). At C20 SR show a similar trend as during C21n (S-profile, Figure 9), with higher SR (43 to 68 cm/kyr) to the east (wedge-top) than to the west, where carbonate platform and slope deposition took place with low to moderate SR (17 to 24cm/kyr).

The northern profile between C20 and C19r highlights changes in SR west of the oblique thrust front (Boltaña and Balzes structures). The N-S orientation of the profile between GA and IS (Figures 2, 9 and 10), perpendicular to the western Pyrenees structures, allows clear observation of the expected SR for a

transition between forebulge, foredeep and wedge-top. In its northern edge, SR reach close to their highest values of 95-104 cm/kyr. To the east of the oblique front (Balzes Anticline) relatively high SR (50 cm/kyr) are obtained from carbonate platform deposits in the SM section in Southern Jaca (Figures 9 and 10c). These carbonate platform deposits display a fan-like geometry related to a syntectonic progressive unconformity linked to the growth of the Balzes anticline (Rodríguez-Pintó *et al.*, 2016). During C19n Southern Jaca shows its maximum SR (41 and >23 cm/kyr) close to the proximal foredeep values for Northern Jaca (53 cm/kyr) and the wedge-top (51 cm/kyr in Ainsa). Thus, during C19, the former distal foreland was incorporated into the foredeep, as deduced from a threefold increase in SR in SM (from C20n to C19r), and double in IS (from C19r to C19n). This part of the foredeep still remained as a carbonate platform because of its protected location from clastic inputs (Figures 9 and 10d).

The transition from Lutetian to Bartonian in Southern Jaca shows an abrupt decrease in the SR (from 41 to >10 cm/kyr) coinciding with the passage from foredeep to a wedge-top situation.

During the Bartonian (between 38.0 - 41.3 Ma) the whole area becomes incorporated into the wedge-top depozone, on top of the Gavarnie-Sierras Exteriores thrust sheet. The Bartonian emplacement of Sierras Exteriores thrust sheet is deduced from the growth of N-S oriented anticlines in the Serres Marginals area (Castelltort *et al.*, 2003; Millan *et al.*, 1994; Poblet & Hardy, 1995) before ramp development during the Oligocene (Labaume & Teixell, 2018). Immediately following the transition to wedge-top, SR reach their highest values (105-115 cm/kyr) in northern Jaca basin. However, in general, SR show a sustained decreasing trend as expected for basins incorporated onto the wedge-top.

A possible reason for the high SR in the wedge-top (Ainsa during Lutetian and Northern Jaca Bartonian to Priabonian) is as the deformation propagates toward the foreland, a new frontal thrust (or its related anticline) does not immediately produce a new proximal foredeep depozone with a relatively higher SR. The sustained moderate-to-high SR during the initial wedge-top situation may be associated with the structural arrangement of the AOZ and front of Sierras Exteriores thrust sheet, with thin-skinned cover units that are deformed in a thrust-flat position with horizontal displacement and uplift mainly restricted to the frontal anticline axes (Figure 11). In this wedge-top depozone, regional subsidence related to the load from the emplacement of basement units in the axial zone (Figure 2b) is not reduced or counteracted by the thrust sheet uplift (Figure 11), keeping SR higher in the synclines and lower in the anticlines.

Basinward migration of depocenters due to shelf clinoform progradation during regressive conditions

A feature observed in four of the profiles illustrated in Figure 9 is an important increase in SR associated with the deposition of shallowing-upwards clastic shelf and deltaic successions (*e.g.,* C20r to C20n at MD or C18r and C19n in GA and YB). Conversely, when deltaic complexes grade upwards to subaerial sediments, a reduction in SR occurs. The first increasing and later decreasing trend in SR is likely related to the shelf clinoform progradation (Figure 12a) and coeval basinward displacement of the boundary between underfilled (below sea level) and overfilled (above sea level) accommodation areas (Catuneanu, 2017). These kinds of progradational shelves are graded margins whose profiles are in equilibrium with depositional and erosional processes operating within each environmental regime (Ross *et al.*, 1994). They display a sigmoidal shape where the largest sediment accumulation takes place in the foreset environments (Alexander *et al.*, 1991; Kuehl *et al.*, 1986; Walsh *et al.*, 2004), which in progradational episodes are expanded, developing accretionary active clinoforms (Patruno & Helland–Hansen, 2018). In regressive and progradational settings, the topsets are overfilled accommodation domains which are close to equilibrium with the base level. Thus, SR in topsets will be mainly controlled by relative sea level (base-level) changes. In the foreset, the accommodation is directly related to the water depth of the marine basin (Figure 12a), and it could be increased or reduced by relative sea level variation. Therefore, SR in prograding foresets is higher than in the topset because here, in addition, the depth of the marine basin is added. In the bottomset SR are usually lower than in the foreset (Figure 12a). Despite that typically both sub-environments share a similar accommodation, the reduced supply of sediments (since they are located in an underfilled accommodation area) diminishes SR in the bottomset.

In the S-profile (Figure 9), the basinward migration of the Ainsa-relative depocenter can be directly linked to a clastic shelf—from C20r, to C19r in the MD log (Figures 9, 10b and 10c). During C20r low SR (21 cm/kyr) are related to carbonate slope settings. At chron C20n, the clastic input arrives to the area, filling the basin trough (close to 500 m deep; Pickering & Corregidor, 2005), first with deep-marine sediments and then with shallow water delta front and shelf facies. The introduction of this clastic sediment is associated with a sharp increase in SR (from 21 to 68 cm/kyr). During C19r, as the Sobrarbe deltaic complex progrades NW, the MD log is no longer located in the foreset, but rather in the topset area. This vertical evolution from foreset to topset in the MD log is associated with an SR reduction (from 68 to 24 cm/kyr). At this stage, the depocenter in Ainsa has migrated westwards (CM log, 45 cm/kyr), as sketched in Figure 12b.

In a similar way, in Northern Jaca (YB log) there is a well-documented increase-to-decrease of the SR related to the Sabiñánigo and Belsué-Atarés deltaic progradation, from C19n to C17r (N-profile, Figure 9). Deltaic foreset progradation during C18r and C18n show high SR (105 cm/kyr and 115 cm/kyr respectively), while in previous (deep sea bottomset) and later stages (topset fluvial and alluvial) SR are

lower (53 cm/kyr). The high SR recorded here is also related to the infill of a marine basin with water depths of several hundreds of meters during clastic shelf progradation.

Contrasting SR during C21 are also observed between the Tremp-Graus (ES log, >30 cm/kyr), showing a shallowing-upward trend as a result of the progradation of a clastic shelf, and the Ainsa and Southern Jaca carbonate platform and slope environments (SR between 3 and >12 cm/kyr).

Uniformization of SR and widening of depocenters due to transgressive conditions

During the latest Lutetian (C19n) we observe an exceptional uniformization of the SR (between 53 and >23 cm/kyr) in both Ainsa and Jaca areas (Figures 9 and 10d). This resulted from a drastic decrease in SR in the Northern Jaca depocenter and an increase in SR in Ainsa and Southern Jaca. Because Chron C19n is relatively short (0.234 Myr, Gradstein *et al.*, 2012) the averaged SR may reflect short-term variations on sediment supply and/or accommodation due to relative sea level or subsidence variations. In Ainsa, a significant part of C19n is represented by the deposition of the Buil nummulite banks carbonate unit (Callot *et al.*, 2009; Dreyer *et al.*, 1999) (Figure 3) embedded between highly progradational clastics of the Sobrarbe deltaic complex (Dreyer *et al.*, 1999, Grasseau *et al.*, 2019). This unit records a transgression larger than 12 km (Grasseau *et al.*, 2019) and a landward displacement of the boundary between underfilled and overfilled accommodation areas. This carbonate platform deposition above and below regressive deltaic complexes implies an Accommodation/Sediment Supply ratio (A/S) higher than that deduced for the long-term general regressive trend of the TJB infill. This relative high A/S may be responsible for trapping more clastic sediments in the topset area. In this situation, clastics are only able to fill the accommodation space in the proximal areas (Figure 12c), resulting in reduced foresets if present (draping passive clinoforms in Patruno & Helland–Hansen, 2018) and delivering less sediment to deep areas. As a result, in the LS log at Tremp-Graus there are higher SR than for the subsequent stages (Figures 9 and 10d). In Southern Jaca, sediment-starved cleaner waters than for Northern Jaca and Ainsa favored higher SR in the carbonate platform. The increase in accommodation in Southern Jaca at this stage can be attributed to the incorporation of the area into the foredeep as the plate flexure advanced southwards.

During Chron C20r SR were relatively uniform when compared with previous and later regressive episodes (S-profile, Figure 9). This period also shows a transgressive trend as marked by the vertical evolution from non-marine to transitional and finally marine carbonate platform deposits in the ES log.

Long-term depocenter in Northern Jaca and Ainsa

As indicated in the previous sections, we have documented a long-term persistent depocenter in Northern Jaca (Figures 7, 9, and 10). This depocenter accumulated a thick succession of deep marine

sediments during Lutetian and early Bartonian times (from before 43.5 to *ca*. 40.8 Ma). The progradation of a graded clastic shelf (Figure 12a) as deduced from the observations in the Ainsa Basin (S-Profile, Figure 9) cannot explain the presence of this depocenter. This configuration implies a high subsidence area in Northern Jaca that accommodated higher SR in deeper bathymetries than the more proximal and shallow marine areas (Ainsa and Tremp-Graus), which were accompanied by a high clastic input. The high subsidence can be directly related to the proximal foredeep depozone situation of Northern Jaca, during the Lutetian (N-profile, Figure 9) associated with its location in the footwall and close to the deformation front (Figure 10). Considering the fluviodeltaic and slope complexes in Tremp-Graus-Ainsa as the main feeders of the Northern Jaca area (Figure 10) (Mutti *et al.*, 1985; Mutti, 1992), a high clastic sediment flux toward deep marine areas in the context of an out-of-grade or erosional margin (Ross *et al.*, 1994), is needed to produce the resulting high SR (Figure 12d). This sediment flux from areas where SR were lower (Figure 10) implies erosion and/or bypass in the foresets. In the Ainsa slopes, these two processes have been documented as related to slope instability (sliding and slumping) and to the erosional and sediment transport capacity of turbidity currents, both operating at a variety of scales and frequencies. These resulted in turbidite channel complexes of the mixed erosional-depositional type (*sensu* Mutti & Normark, 1987; 1991), large-scale canyons (Mutti *et al.*, 1985), or submarine truncation surfaces (Arbués *et al.*, 2011). This large-scale out-of-grade period deduced for the whole Lutetian shows higher-frequency cycles of graded margin progradation-outbuilding that progressively oversteepening until reaching the situation of an out-of-grade margin with upbuilding in deep marine areas; finally restoring the conditions to a graded shelf progradation (as developed by Ross *et al.*, 1994). This cyclic behavior of the clastic margin has been described for the northern Ainsa Basin by Mutti *et al.* (1985) and Arbués *et al.* (2011). Previous studies point to high rates of clastic sediment input, seismicity, and tectonically-driven oversteepening as in Odonne *et al.*, (2011), or, periods of relative sea level fall and subaerial exposure of the shelf (Castelltort *et al.*, 2017) as an influence on the oversteepening, destabilization and sediment transfer across the slope. Thus, during the Lutetian (*ca*. 40.8 Ma) the Northern Jaca depocenter received deep water deposition related to the periodically out-of-grade margins, whereas, in Southern Ainsa the deposition records dominant graded shelf progradation episodes.

During the Bartonian, Northern Jaca continued as the main depocenter. At C18r, the clastic shelf progradation reached the Jaca basin, while substituting the deep marine sedimentation in Northern Jaca and the carbonate platforms in Southern Jaca (Figures 9 and 10). At this time, the Sabiñánigo Delta prograded onto a deep water area (Northern Jaca) and the near-complete infill of a water column of several hundreds of meters resulted in high SR associated with the graded shelf progradation (Figures 9, 10, and 12a). Following a transgressive episode on top of Sabiñánigo sandstone (Puigdefàbregas, 1975),

peak SR of 115 cm/kyr occurred in Northern Jaca during Chron C18n (170 cm/kyr—if subchron C18.1r is considered), related to the graded shelf progradation of the Belsué-Atarés deltaic Formation.

During the latest Bartonian (C17r), the continuous progradation toward the southwest of the coastal systems in Northern Jaca resulted in alluvial deposition in the YB log, a progressive lowering of SR, and the obscuring of the depocenter during the Priabonian (C17n) coeval to the homogenization of the SR in the Jaca and Ainsa sub-basins.

In Southern Ainsa, a relative depocenter between Chrons C20n and C18r (Figure 9), shows SR that first increases and then decreases, an evolution that can be explained with the graded clastic shelf progradation model (Figure 12a). The arrival of the clastic systems to the MD log coincided with a major increase in SR from C20r to C20n. Noticeably, a coeval increase in SR also affected the Southern Jaca carbonate platforms, which were sheltered from clastic input. This fact points to a widespread accommodation increase (Southern Jaca and Ainsa). The sum of the generalized accommodation increase and the almost complete infill of the depocenter by the prograding shelf resulted in a major increase in SR. At the end of the Lutetian (C19r) the non-marine strata of the Escanilla formation had already filled most of the southern Ainsa sub-basin (Figures 9 and 10). Nevertheless, the Ainsa relative depocenter was still present during C19n and C18r; and this persistence required other factors in addition to the graded clastic shelf progradation.

Unexpected high sedimentation rates in non-marine settings (local tectonics, sediment load, salt withdrawal and regional subsidence distribution)

The graded shelf progradation model (Figure 12a) predicts a decrease in SR at the transition from foreset to topset settings. However, in a wedge-top context, the topset fluvial areas at MD, CM, and OL logs in Ainsa during C19n and C18r, or YB during C17, were still depocenters (Figures 9 and 10) with SR higher or similar to adjacent downstream areas that were developing deltaic progradation (Southern Jaca). SR were also higher than areas upstream in Graus-Tremp with non-marine sedimentation. A key local factor here was the synchronous tectonic growth of adjacent structures (Boltaña, Balzes, and Mediano anticlines in the Ainsa sub-basin and Oturia thrust and Yebra de Basa anticline in the Jaca sub-basin, see Figures 2b and 10), which could have influenced the local subsidence, sediment supply, or clastic sediment routing or trapping.

At the end of the Lutetian (C19) most of the southern Ainsa basin filled with continental sediments of the Escanilla formation. This fluvial system was substituted at a very short distance westward by the Guara

Formation carbonate platforms of Southern Jaca (S-profile, Figure 9). This transition from fluvial and alluvial sediments to carbonate platforms cannot be physically traced due to the present-day interruption of the outcrops of that age along the Boltaña and Balzes anticlines (Figure 2). The synsedimentary development of these anticlines from middle Lutetian to lower Bartonian is demonstrated by growth strata and also by paleocurrent patterns (Arbués *et al.*, 2011; Dreyer *et al.*, 1999; Michael, *et al.*, 2014; Muñoz *et al.*, 2013; Mutti *et al.*, 1988; Puigdefàbregas, 1975; Rodríguez-Pintó *et al.*, 2016; Soto & Casas, 2001, among others). In the Ainsa basin, the anticline growth forced the clastic systems (turbidite units first, followed by deltaic and alluvial units) to adopt a NNW direction that paralleled the anticlines (Figures 10c and d). During the growth episodes, in the transition from Lutetian to Bartonian, the originally submarine buried anticlines shoaled in the southern Ainsa basin and produced a temporary barrier, preventing the transit of the clastic sediments towards the west (Bentham *et al.*, 1992; Dreyer *et al.*, 1999; Moss, 2005). As a result, detrital sediments accumulated in the Ainsa basin and carbonate sedimentation persisted in Southern Jaca (Figure 9). The paleogeographic barrier promoted clastic funneling and an increased transfer of clastics northwards to Northern Jaca Basin (Figure 10d). The fold growth of Boltaña and Balzes, together with the Mediano anticline (Figures 2a, 2b and 10), resulted in a synsedimentary intermediate syncline structure, the Buil syncline (Figure 2b), which established a local depocenter in the center of the Ainsa basin (Figure 9). The relative high SR for the Buil syncline during C19n and C18r (Figures 9, 10d, and 10e) may be the result of interference and feedback among different tectonic and sedimentary factors as shown in Figure 13. The anticline growth in Boltaña-Balzes generated a barrier for clastic transfer and the location of a simultaneous clastic trough along the Buil syncline (Figure 13c). The Buil syncline had high SR that caused local sediment load which increased local subsidence, favoring the migration of Keuper salts from the syncline to the adjacent anticlines (Figure 13 a, b, and c) and diapiric structures (Clamosa and probably Naval)— similar to the models presented by Ge *et al.* (1997). Salt migration could reinforce the anticline growth and generate a local salt withdrawal depocenter in the Ainsa Basin. The growth of evaporite-cored anticlines in this region linked to tectonic and sediment load driven salt migration was pointed out by Holl & Anastasio (1993), Santolaria *et al.* (2016) and Soto *et al.* (2002) among others. This situation ends during Chron C18r, when the clastic flux was transferred to the SE over the Boltaña and Balzes anticlines, arriving to Southern Jaca Basin (Figures 9, 10e, and 10f).

In the Jaca Basin, during Bartonian and Priabonian, there is a thrust front located to the south at Sierras Exteriores, which developed synchronously with some the thrusts and thrust-related folds to the north (Monte Perdido system, Oturia, and Jaca, Figures 2a, 2b, and 10). The evolution of the thrusts located north of the Jaca Basin (Figure 10) produced a southwards-migrating uplift during the Lutetian, Bartonian

and Priabonian that resulted in a clastic supply increase of northern origin and the incorporation of earlier foredeep strata (Hecho group turbidites) into the uplifted wedge-top source area (Roigé *et al.*, 2016; Labaume *et al.*, 2016).

The influence of northern provenance systems is first observed in middle Lutetian Jaca turbiditic unit paleocurrents (Figure 10c) and extends to at least C17r, interfering with the axial Tremp-Graus-Ainsa clastic sediment routing system. During C17 SR show a significant increase towards north across the Jaca Basin, with much higher values in YB where alluvial sedimentation was taking place than in BL (progradational shallow marine deltaics). This contrasts with the expected SR for prograding shelves, lower in non-marine sediments and higher in prograding clinoforms. We argue this distribution of SR, as seen in the Depozones section, is the response to the tectonic subsidence related to the load of basement-involving thrust sheets (Gavarnie-Oturia and Sierras Exteriores) to the north, producing a northwards dipping regional flexure. The increased clastic supply resulting from the merging of the axial and the northern provenance systems produced a southwestwards progradation of the detrital systems. This resulted in a progressive continentalization, restricting the marine sedimentation to the southern the Jaca Basin.

The extremely high SR associated with the evolution from the Belsué-Atarés delta to the Santa Orosia alluvial fan deposits during C18 (Figures 9 and 10f) is interpreted as regional subsidence due to load of basement thrusts, and the progradation of the clinoforms of the Belsué-Atarés deltaic system onto a deep basin floor.

Evolution of the TJB and sedimentation rates: final remarks

The broad view of the whole TJB is that over a period of about 10 Myr, continuous sedimentation led to a vertical aggradation ranging from 0.9 km (Southern Jaca) to 3.7 km (Northern Jaca). The subsidence required to sustain long-term accommodation in the basin resulted from the combined contribution of tectonic and sediment loads. Sea level rise and fall cycles with amplitudes of a few tens of meters (Miller *et al.*, 2005), had no significant influence at this scale of observation. The generalized regressive pattern resulted from an amount of clastic supply able to progressively fill the basin and evolve from a partially underfilled to an overfilled accommodation setting.

The initial basin topography for the Temp-Graus Basin was inherited from the Montsec-Peña Montañesa thrust sheet geometry (Figures 2 and 10) emplaced during the Ypresian/lowermost Lutetian. The thrust emplacement generated a topographic high on top of the thrust sheet (Tremp-Graus basin / wedge-top depozone). Immediately adjacent (west) of the newly formed Tremp-Graus wedge-top basin was the

Ainsa Basin and Northern Jaca Basin proximal foredeep depozone that extended southwards to the topographic high at the southern foreland basin margin (Southern Jaca Basin / distal foreland depozone). Thus, the trough that received most of the clastic sediments during the Lutetian (Ainsa-Jaca) had a steep gradient associated with the initial proximal foredeep situation of the Northern Jaca Basin (Figures 10 and 12d). In the Northern Jaca foredeep, deep marine sedimentary systems were fed from oversteepened out-of-grade margins. The depocenter extended toward the SE to include the Ainsa area, in spite of being progressively incorporated into the wedge-top.

A secondary shifting depocenter was associated with the progradation of the graded clastic shelf clinoforms parallel to the trough axis. This secondary depocenter was originally located on the wedge-top depozone (first in Tremp-Graus, and then in the Ainsa Basin) and migrated toward the foredeep at a slower rate than the deformation front, reaching the Northern Jaca area at the time it was already incorporated in the wedge-top depozone (Bartonian). The out-of-phase evolution of foreland depozones with respect to the prograding clastic shelf wedge has resulted in complex SR that are not diagnostic of a specific foreland setting.

From the evolution of SR, the distribution of facies belts, and the depocenter position, we distinguish two main stages of the TJB evolution: the Lutetian (C21n – C19n, from 47.8 to 41.2 Ma) and the Bartonian-Priabonian stages (C18r – C17n, from 41.2 to 37.0 Ma).

The Lutetian Stage was characterized by variable SR in a highly compartmentalized basin. From east to west, lower SR or erosion in the Tremp-Graus Basin (10 cm/kyr – >30 cm/kyr) shift to higher rates in the Ainsa Basin (4 cm/kyr – 68 cm/kyr), and to much higher rates in the Northern Jaca Basin (53 cm/kyr – 101 cm/kyr). During this stage, the Southern Jaca Basin started as a distal foreland depozone with low to moderate values (3 cm/kyr – 24 cm/kyr) and later (C19), was progressively incorporated into the foredeep with moderate to high SR (>23 cm/kyr – 50 cm/kyr) (Figures 9 and 10d). The lowest SR are located in the eastern proximal Tremp-Graus area and the Southern Jaca Basin, associated with non-marine (wedge-top environment) and carbonate platform facies (forebulge environment), whereas the highest SR correspond to clastic turbidites and shelf foresets in Ainsa and Jaca. In the Northern Jaca basin, a persistent major depocenter accumulated a thick succession of deep sea sediments in the foredeep depozone under an important clastic input related to the out-of-grade situation of the shelf margin. In the Ainsa Basin, the initial wedge-top situation shows a well-developed wedge-like section, probably inherited from a prior foredeep formed during the emplacement of the Montsec thrust sheet earlier during Ypresian. High SR during the wedge-top stage can be associated with a period of tectonic transport over a thrust flat (Figure 11) if regional subsidence due to basement thrusting to the north was not counterbalanced by local thrust sheet uplift.

At the beginning of the Bartonian Stage (41.2 Ma) the whole area was incorporated on top of the Gavarnie-Sierras Exteriores thrust sheet (Figures 2b and 10e) as a wedge-top depozone. From east to west SR were low in Tremp-Graus Basin (4 cm/kyr – 13cm/kyr); shifting to moderate rates in the Ainsa Basin (21 cm/kyr – >29 cm/kyr); high rates in Northern Jaca Basin (>31 cm/kyr – 115 cm/kyr); and moderate values in the Southern Jaca Basin (10 cm/kyr – 26 cm/kyr). At this time, the northwestwards migration of the clastic shelf-related depocenter ended with its merging with the persistent depocenter located in the Northern Jaca Basin. This new scenario was characterized by a more uniform SR and the lack of tectonic barriers (*e.g.,* Boltaña and Balzes anticlines). The clastic transfer systems reached the Southern Jaca Basin producing a displacement of the carbonate platform toward the southwest (*e.g.,* Santo Domingo member, Silva-Casal *et al.*, 2019). During the Bartonian and Priabonian, synchronous thrusting occurs at the southern front (Sierras Exteriores) and in the north (Sierras Interiores). A wedge-like section typical of a foredeep developed due to the high subsidence of the northern sector, linked to its footwall position in relation to the northern thrusts and the load of basement-involving units in the axial zone.

As the TJB developed in a foreland basin system, tectonics had the primary role driving subsidence. The contribution of the sediment load to the total subsidence enhanced locally by a feedback process in which salt withdrawal from sediment-filled synclines migrated to adjacent anticlines (figure 13). The rising anticlines temporarily confined a part of the basin, producing a relative depocenter. This explains the relative high SR observed in the non-marine Escanilla formation of the Ainsa Basin.

CONCLUSIONS

We calculated sedimentation rates (SR) for the South-Pyrenean foreland TJB using a magnetostratigraphic time resolution (time lapse) of nearly 10 Myr, ranging from Lutetian to Priabonian times (47.8 to 37.0 Ma). We conclude that despite the fact that subsidence-related accommodation is the major control over long-term SR, higher-frequency SR over the million-year time range may not reflect the expected trends for tectonic divisions of foreland systems into wedge-top, foredeep, and distal foreland depozones. This divergence from expected SR is in part due to strong lateral changes in the foreland basin due to the differential thrust propagation between central and western Pyrenees during the Lutetian which moved the deformation front very close to the forebulge in southern Ainsa basin. In addition, tectonic load distribution and timing may play a role. The repeated stacking of tectonic units in the hinterland, with basement-involved units in the axial zone, contributed to a much higher load than the frontal thin-skinned structures of the chain, resulting in higher subsidence and SR in areas of the wedge-top depozone. The tectonic transport along a thrust flat in the initial stages of the wedge-top development had a minor contribution to tectonic load and relative vertical movements compared to later stages of thrust ramping and wedge-top uplift.

An additional source of subsidence comes from salt-withdrawal or migration processes during fold growth in the wedge-top depozone. These processes may cause accommodation and SR higher than predicted for the setting, such as for example in Southern Ainsa during Chrons C18n and C18r, and Northern Jaca during C18r to C17r.

Subsidence-driven accommodation is the main influence over SR, but then accommodation must be accompanied by clastic sediment supply or carbonate production to fill the available space. At any point in a sedimentary basin, maximum SR are attained when the space between the basin floor and the base level is fully occupied with sediments, leading to an overfilled accommodation situation. Thus, SR in overfilled accommodation areas will be controlled by accommodation, whereas in underfilled accommodation areas the main control will be the sediment supply or production.

Under regressive conditions, the graded shelf progradation model predicts that the maximum SR will be obtained in the foreset areas where sediments accumulate on clinoforms, from basin floor to sea level. This scenario is exemplified in Tremp-Graus during Chron C21, in Ainsa during C20n and 19r, and in Northern Jaca during C18. The resulting depocenter is mobile and migrates basinward together with the boundary between the underfilled and overfilled accommodation areas. Topset areas (if present) will show lower SR that are directly controlled by the accommodation variations. Bottomset areas will display

lower SR than the foresets since they share the same accommodation but in the bottomset it is underfilled.

During accretionary transgressive episodes maximum SR will be obtained at the topset area since the landwards migration of the underfilled/overfilled accommodation boundary will be progressively located landwards, and the reduced amount of sediments will reach the underfilled slope (foreset) and basin floor (bottomset). This scenario is exemplified in Tremp-Graus during Chron C20r, and in Ainsa during C19n. However, in the case of highly unstable, erosional, or bypassing foreset slopes, resulting from tectonically induced subsidence and slope steepening (out-of-grade margins) a high amount of sediment will reach deep marine areas, producing high SR, such as in Northern Jaca during C20 to C18r. High SR would persist throughout time if there is a high bathymetry or subsidence rate able to keep this area within underfilled accommodation conditions.

Underfilled or overfilled accommodation condition of an area is crucial for controlling SR trends. It is possible to envisage for instance, high SR in the wedge-top depozones and low SR where foredeep development is expected. This makes the distinction between wedge-top, proximal foredeep, and distal foreland depozones based only on SR potentially misleading. Additional analysis including depositional architecture, facies analysis and relative timing of tectonic structures is required. Further research including subsidence analysis of different logs and forward computer and analogue modeling will help to strengthen, support, or refute the ideas and hypotheses presented in this work.

REFERENCES

Alexander, C.R., DeMaster, D.J., Nittrouer, C.A., (1991). Sediment accumulation in a modern epicontinental-shelf setting: The Yellow Sea. *Marine Geology, 98*, 51–72.

Allen, P.A., Crampton S.L., Sinclair H.D. (1991). The inception and early evolution of the north alpine foreland basin, Switzerland. *Basin Research* 3:143–163.

Angevine, C. L., Heller, P. L., & Paola, C. (1992). *Quantitative sedimentary basin modeling*. Universitat de Barcelona.

Arbués, P., Butillé, M., López-Blanco, M., Marzo, M., Monleón, O., Muñoz, J. A., & Serra-Kiel, J. (2011). Exploring the relationships between deepwater and shallow-marine deposits in the Aínsa piggy-back basin fill (Eocene, South- Pyrenean Foreland Basin). *Post-Meeting Field Trips Guidebook, 28th IAS Meeting*, 199–240.

Bally, A. W. (1984). *Structural styles and the evolution of sedimentary basins*. AAPG Short Course.

Barnolas, A. & Pujalte, B. (2004). La Cordillera Pirenaica. In: Vera JA (ed) Geología de España, Instituto Geológico y Minero de España - Sociedad Geológica de España, 231–343

Barnolas, A., Larrasoaña, J.C., Pujalte, V., Schmitz, B., Sierro, F.J., Mata, M.P., van den Berg, B.C. J., Pérez-Asensio, J.N., Salazar, A., Salvany, J.M., Ledesma, S., García-Castellanos, D., Civis, J. & Cunha, P. (2019). Alpine foreland basins. A: "The geology of Iberia: a geodynamic approach". Berlín: Springer, 7-59. DOI10.1007/978-3-030-11190-8_2

Barsó, D. (2007). *Análisis de la procedencia de los conglomerados sinorogénicos de La Pobla de Segur (Lérida) y su relación con la evolución Tectónica de los Pirineos centro-meridionales durante el Eocenomedio-Oligoceno*. PhD thesis. Universitat de Barcelona. 209 pp.

Beamud, E. (2013). *Paleomagnetism and Thermochronology in Tertiary Syntectonic Sediments of the*

South-Central Pyrenees : Chronostratigraphy , Kinematic and Exhumation Constraints. PhD thesis. Universitat de Barcelona. 250 pp.

Beamud, E., Garcés, M., Cabrera, L., Muñoz, J. A., & Almar, Y. (2003). A new middle to late Eocene continental chronostratigraphy from NE Spain. *Earth and Planetary Science Letters*, *216*(4), 501–514. DOI: 10.1016/S0012-821X(03)00539-9

Beamud, E., Muñoz, J. A., Fitgerald, P.G., Baldwin, S. L., Garcés, M., Cabrera, L., & Metcalf, J. R. (2011). Magnetostratigraphy and detrital apatite fission track thermochronology in syntectonic conglomerates: constraints on the exhumation of the South-Central Pyrenees. *Basin Research, 23*, 309-331. DOI: 10.1111/j.1365-2117.2010.00492.x

Beaumont, C., Muñoz, J.A., Hamilton, J., Fullsack, P. (2000). Factors controlling the Alpine evolution of the central Pyrenees inferred from a comparison of observations and geodynamical models. *Journal of Geophysical Research* 105: doi: 10.1029/1999JB900390. issn: 0148-0227.

Bentham, P. A. (1992). *The tectono-stratigraphic development of the western oblique ramp of the South-Central Pyrenean Thrust System, Northern Spain*. PhD thesis. University of Southern California.

Bentham, P. A., & Burbank, D. W. (1996). Chronology of Eocene foreland basin evolution along the western oblique margin of the South-Central Pyrenees. In P. F. Friend & C. J. Dabrio (Eds.), *Tertiary Basins of Spain: The Stratigraphic Record of Crustal Kinematics* (pp. 144–152). New York: Cambridge University Press.

Berástegui, X., Losantos, M., Muñoz, J.A., Puigdefàbregas, C. (1993) *Tall geologic del Pirineu Central 1:200.000.* Servei Geològic de Catalunya-Institut Cartogràfic de Catalunya, Barcelona.

Bentham, P. A., Burbank, D.W. & Puigdefàbregas, C. (1992). Temporal and spatial controls on the alluvial architecture of an axial drainage system: late Eocene Escanilla Formation, southern Pyrenean foreland basin, Spain. *Basin Research, 4*, 335-352.

Callot, P., Odonne, F., Debroas, E. J., Maillard, A., Dhont, D., Basile, C. & Hoareau, G. (2009). Three-dimensional architecture of submarine slide surfaces and associated soft-sediment deformation in the Lutetian Sobrarbe deltaic complex (Ainsa, Spanish Pyrenees). *Sedimentology*, *56*, 1226–1249.

Cámara, P., & Klimowitz, J. (1985). Interpretación Geodinámica de la vertiente centro-occidental surpirenaica (Cuencas de Jaca - Tremp). *Estudios Geologicos*, *41*, 391–404. DOI: 10.3989/egeol.85415-6720

Cant, D. J., & Stockmal, G. S. (1989). The Alberta foreland basin: relationship between stratigraphy and Cordilleran terrane-accretion events. *Canadian Journal of Earth Sciences*, *26*(10), 1964–1975. DOI: 10.1139/e89-166

Castelltort, S., Guillocheau, F., Robin, C., Rouby, D., Nalpas, T., Lafont, F., Eschard, R., (2003). Fold control

on the stratigraphic record: a quantified sequence stratigraphic study of the Pico del Aguila anticline in the south-western Pyrenees (Spain). *Basin Research.* 15, 527–551. DOI: 10.1046/j.1365-2117.2003.00218.x.

Castelltort, S., Honegger, L., Adatte, T., Clark, J. D., Puigdefàbregas, C., Spangenberg, J. E., … Fildani, A. (2017). Detecting eustatic and tectonic signals with carbon isotopes in deep-marine strata, Eocene Ainsa Basin, Spanish Pyrenees. *Geology*, *45*(8), 707–710. DOI: 10.1130/G39068.1

Catuneanu, O., (2017). Sequence Stratigraphy: Guidelines for a Standard Methodology. In: Michael Montenari (Ed.) *Stratigraphy & Timescales, Volume 2,* 2-57. Elsevier. DOI: 10.1016/bs.sats.2017.07.003

de Federico, A. (1981). *La sedimentación de talud en el sector occidental de la Cuenca Paleógena de Aínsa.* Barcelona: Universitat Autònoma de Barcelona. Publicaciones de Geología 12.

DeCelles, P. G., & Giles, K. A. (1996). Foreland basin systems. *Basin Research*, *8*(2), 105–123. DOI: 10.1046/j.1365-2117.1996.01491.x

DeCelles, P.G. (2012). Foreland basin systems revisited: variations in response to tectonic settings. In: Busby, C. & Azor-Pérez, A. (eds.), *Tectonics of sedimentary basins: Recent advances*. (pp. 405-426).

Donselaar, M. E., & Nio, S. D. (1982). An Eocene Tidal Inlet Washover Type Barrier-Island Complex in the South Pyrenean marginal Basin, Spain. *Geologie En Mijnbouw*, 343–353.

Dorobek, S. (1995). Synorogenic carbonate platforms and reefs in foreland basins: controls on stratigraphic evolution and platform/reef morphology. In: Stratigraphic Evolution of Foreland Basins. SEPM Special Publication nº 52. 128-147. DOI: 10.2110/pec.95.52.0127

Dreyer, T., Corregidor, J., Arbués, P., & Puigdefàbregas, C. (1999). Architecture of the tectonically influenced Sobrarbe deltaic complex in the Ainsa Basin, northern Spain. *Sedimentary Geology*, *127*(3–4), 127–169. DOI: 10.1016/S0037-0738(99)00056-1

Einsele, G. (2000). *Sedimentary Basins: Evolution, Facies, and Sediment Budget*. Springer Science & Business Media, 792 pp.

Erdos, Z.; Huismans, R.S.; van der Beek, P. (2019). Control of increased sedimentation on orogenic fold-and-thrust belt structure – insights into the evolution of the Western Alps. *Solid Earth, 10,* 391–404. DOI: 10.5194/se-10-391-2019

Fernández-Bellón, O. (2004). *Reconstruction of geological structures in 3D. An example from the Southern Pyrenees.* PhD thesis. Universitat de Barcelona. 321 p.

Garcés, M., López-Blanco, M., Valero, L., Beamud, E., Pueyo-Morer, E., & Rodríguez-Pintó, A. (2014). Testing orbital forcing in the Eocene deltaic sequences of the South-Pyrenean Foreland Basins. European Geosciences Union General Assembly. Viena.

Garcés, M., López-Blanco, M., Valero, L., Beamud, E., Oliva, B., Vinyoles, A., Arbués, P., Cabello, P., & Cabrera, L. (2020). Sedimentary trends, shifts and breaks across the South-Pyrenean Foreland System. *Marine and Petoleum Geology. 113.* DOI: 10.1016/j.marpetgeo.2019.104105

Garrido-Mejias, A. (1968). Sobre la estratigrafia de los conglomerados de Campanué (Santa Liestra) y formaciones superiores del Eoceno (extremo occidental de la cuenca de Tremp-Graus, Pirineo Central, provincia de Huesca). *Acta Geológica Hispánica*, *3*(2), 39–43.

Ge, H., Jackson, M. P. A., & Vendeville, B.C. (1997). Kinematics and dynamics of salt tectonics driven by progradation. *AAPG Bulletin*, *81*(3), 398-423.

Gradstein, F. M., Ogg, J. G., Schmitz, M. D., & Ogg, G. M. (2012). *The Geological Time Scale*. Amsterdam: Elsevier.

Grasseau, N. (2016). *Architecture, dynamique et modélisation sismique synthétique d'un système fluvio-deltaïque syntectonique.* PhD thesis. Université Bordeaux Montaigne, Universitat de Barcelona.

Grasseau, N., Grélaud, C., López-Blanco, M., & Razin, P. (2019). Forward seismic modeling as a guide improving detailed seismic interpretation of deltaic systems: Example of the Eocene Sobrarbe delta outcrop (South-Pyrenean foreland basin, Spain), as a reference to the analogous subsurface Albian-Cenomanian Torok-Nanushuk Delta of the Colville Basin (NPRA, USA). *Marine and Petroleum Geology. 100*, 225–245. DOI: 10.1016/j.marpetgeo.2018.11.010

Hogan, P. J., & Burbank, D. W. (1996). Evolution of the Jaca piggyback basin and emergence of the External Sierra, southern Pyrenees. In P. F. Friend & C. J. Dabrio (Eds.), *Tertiary Basins of Spain: The Stratigraphic Record of Crustal Kinematics* (pp. 153–160). New York: Cambridge University Press.

Holl, J. E., & Anastasio, D. J. (1993). Paleomagnetically derived folding rates, southern Pyrenees, Spain. *Geology*, *21*, 271–274. DOI: 10.1130/0091-7613(1993)021<0271:PDFRSP>2.3.CO;2

Homewood, P., Allen, P. A., & Williams, G. D. (1986). Dynamics of the Molasse Basin of western Switzerland. In *Foreland Basins: International Association of Sedimentologists Special Publication 8* (pp. 199–217). DOI: 10.1002/9781444303810.ch10

Huyghe, D., Castelltort, S., Mouthereau, F., Serra-Kiel, J., Filleaudeau, P. Y., Emmanuel, L., Berther, B., Renard, M. (2012). Large scale facies change in the middle Eocene South-Pyrenean foreland basin: The role of tectonics and prelude to Cenozoic ice-ages. *Sedimentary Geology, 253-254*, 25-46. DOI: 10.1016/j.sedgeo.2012.01.004

Johnson, N. M., & McGee, V. E. (1983). Magnetic polarity stratigraphy: Stochastic Properties of Data, Sampling Problems, and the Evaluation of Interpretations. *Journal of Geophysical Research*, *88*(B2), 1213–1221. DOI: 10.1029/JB088iB02p01213

Kirschvink, J.L. (1980). The least squares lines and plane analysis of paleomagnetic data. *Geophys. J. R. Astron. Soc.*, *62*, 699–718.

Kodama, K. P., Anastasio, D. J., Newton, M. L., Parés, J. M., & Hinnov, L. A. (2010). High-resolution rock magnetic cyclostratigraphy in an Eocene flysch, Spanish Pyrenees. *Geochemistry, Geophysics, Geosystems, 11*, Q0AA07. DOI: 10.1029/2010GC003069

Kuehl, S.A., DeMaster, D.J., Nittrouer, C.A., (1986). Nature of sediment accumulation on the Amazon continental shelf. *Continental Shelf Research, 6*, 209–336.

Labourdette, R. (2011). Stratigraphy and static connectivity of braided fluvial deposits of the lower Escanilla Formation, south central Pyrenees, Spain. *AAPG Bulletin*, *95*(4), 585–617. DOI: 10.1306/08181009203

Labaume, P., Mutti, E. & Seguret, M. (1987). Megaturbidites: a depositional model from the Eocene of the SW-Pyrenean Foreland Basin, Spain. *Geo-Marine Letters, 7*, 91-101.

Labaume, P., Meresse, F., Jolivet, M., Teixell, A. & Lahfid, A. (2016). Tectonothermal history of an exhumed thrust-sheet-top basin: An example from the south Pyrenean thrust belt, *Tectonics*, *35*, 1280–1313, DOI:10.1002/2016TC004192.

Labaume, P. & Teixell, A. (2018). 3D structure of subsurface thrusts in the eastern Jaca Basin, southern Pyrenees. *Geologica Acta*, *14*(4), 477-498. DOI: 10.1344/GeologicaActa2018.16.4.9

Maesano, F.E.; D'Ambrogi, C. (2015). Coupling sedimentation and tectonic control: Pleistocene evolution of the central Po Basin. *Italian journal of Geosciences, 135*(3), 394-407. DOI: 10.3301/IJG.2015.17

Mangin, J. P. (1959-60). Le Nummulitique sud-Pyrénéen à l'Ouest de l'Aragon. *Pirineos*, *51–58*, 1–631.

McFadden, P. L., & McElhinny, N. W. (1990). Classification of the reversal test in palaeomagnetism. *Geophysical Journal International*, *103*(3), 725-729. DOI: 10.1111/j.1365-246X.1990.tb05683.x

Miall, A. D. (1995). Collision-Related Foreland Basins. In: Busby, C. J. & Ingersoll, R. V. (eds.), *Tectonics of Sedimentary Basins* . Backwell Science. 393–424.

Michael, N. A., Whittaker, A. C., Carter, A., & Allen, P. A. (2014). Volumetric budget and grain-size fractionation of a geological sediment routing system: Eocene Escanilla Formation, south-central Pyrenees. *Geological Society of America Bulletin*, *126*(3–4), 585–599. DOI: 10.1130/B30954.1

Millan, H., Aurell, M., & Melendez, A. (1994). Synchronous detachment folds and coeval sedimentation in the Prepyrenean External Sierras (Spain): a case study for a tectonic origin of sequences and systems tracts. *Sedimentology*, *41*(5), 1001–1024. DOI: 10.1111/j.1365-3091.1994.tb01437.x

Miller, K.G., Kominz, M.A., Browning, J.V., Wright, J., Mountain, G.S., Katz, M.E. Sugarman, P.J. Cramer, B.S., Christie-Blick, N. & Pekar, S.F. (2005). The Phanerozoic record of global sea-level change.

Science, 310, 1293–1298.

Mochales, T., Barnolas, A., Pueyo, E. L., Serra-Kiel, J., Casas, A. M., Samsó, J. M., … Sanjuán, J. (2012). Chronostratigraphy of the Boltaña anticline and the Ainsa Basin (southern Pyrenees). *GSA Bulletin*, *124*(7–8), 1229–1250. Retrieved from DOI: 10.1130/B30418.1

Montes, M. J. (2009). Estratigrafía del Eoceno-Oligoceno de la Cuenca de Jaca. Sinclinorio del Guarga*. Coleccion de Estudios Altoaragoneses*, *59*, 1-355.

Moss, J. (2005). *Tectonic controls on eocene deltaic architecture, jaca basin, Spanish pyrenees.* PhD. Durham University. 351pp.

Moody, J. D., Pyles, D. R., Clark, J. D., & Bouroullec, R. (2012). Quantitative outcrop characterization of an analog to weakly confined submarine channel systems: Morillo 1 member, Ainsa Basin, Spain. *AAPG Bulletin*, *96*(10), 1813–1841. DOI: 10.1306/01061211072

Muñoz, J. A., Beamud, E., Fernández, O., Arbués, P., Dinarès-Turell, J., & Poblet, J. (2013). The Ainsa Fold and thrust oblique zone of the central Pyrenees: Kinematics of a curved contractional system from paleomagnetic and structural data. *Tectonics*, *32*(5), 1142–1175. DOI: 10.1002/tect.20070

Mutti, E. (1992). Turbidite sandstones. *AGIP / Instituto di Geologia, Università di Parma.* 275 p.

Mutti, E., Seguret, M. & Sgavetti, M. (1988). *Sedimentation and deformation in the Tertiary sequences of the southern Pyrenees.* Guidebook to fieldtrip 7. American Association of Petroleum Geologists, Mediterranean Basins Conference, Nice.

Mutti, E., Luterbacher, H. P., Ferrer, J., & Rossell, J. (1972). Schema stratigrafico e lineamenti di facies del Paleogene marino della zona centrale sudpirenaica tra Tremp (Catalogna) e Pamplona (Navarra). *Mem. Soc. Geol. Ital.*, *11*(3), 391–416.

Mutti, E. & Normark, W.R. (1987). Comparing examples of modern and ancient turbidite systems: problems and concepts. In: Legget, J.R. and Zuffa, G.G. (eds.). *Marine Clastic Sedimentology: Concepts And Case Studies*. G. Graham and Trotman, London, 1-37.

Mutti, E. & Normark, W.R. (1991). An integrated approach to the study of turbidite systems. In: Weimer, P. and Link, H. (eds.), *Seismic Facies And Sedimentary Processes Of Submarine Fans And Turbidite Systems.* Springer, New York, 75-106.

Mutti, E., Remacha, E., Sgavetti, M., Rosell, J., Valloni, R. & Zamorano, M. (1985). Stratigraphy and facies characteristics of the Eocene Hecho Group turbidite systems, south-central Pyrenees. *In: Milà, M. D. & Rosell, J., eds., 6th European IAS Regional Meeting Excursion Guidebook: Lleida, Institut d'Estudis Ilerdencs.* 519–576.

Nijman, W., & Nio, S. D. (1975). The Eocene Montañana delta. In: Rosell, J.& Puigdefàbregas, C. (eds.), *Sedimentary evolution of the Paleogene South Pyrenean Basin. IAS 9th International Congress*. Nice.

Odonne, F., Callot, P., Debroas, E.-J., Sempere, T., Hoareau, G., & Maillard, A. (2011). Soft-sediment deformation from submarine sliding: Favourable conditions and triggering mechanisms in examples from the Eocene Sobrarbe delta (Ainsa, Spanish Pyrenees) and the mid-Cretaceous Ayabacas Formation (Andes of Peru). *Sedimentary Geology*, *235*(3–4), 234–248. DOI: 10.1016/j.sedgeo.2010.09.013

Oms, O., Dinarès-Turell, J., & Remacha, E. (2003). Magnetic stratigraphy from deep clastic turbidites: An example from the Eocene Hecho group (Southern Pyrenees). *Studia Geophysica et Geodaetica*, *47*(2), 275–288. DOI: 10.1023/A:1023719607521

Patruno, S. & Helland-Hansen, W. (2018). Clinoforms and clinoform systems: Review and dynamic classification scheme for shorelines, subaqueous deltas, shelf edges and continental margins. *Earth-Science Reviews, 185*, 202–233.

Patton, T. L. & O'Connor, S. J. (1988). Cretaceous flexural history of northern Oman Mountain foredeep, United Arab Emirates. AAPG Bulletin 72 (7). 797-807.

Pickering, K. T., & Corregidor, J. (2005). Mass-Transport Complexes (MTCs) and Tectonic Control on Basin-Floor Submarine Fans, Middle Eocene, South Spanish Pyrenees. *Journal of Sedimentary Research*, *75*, 761–783. DOI: 10.2110/jsr.2005.062

Poblet, J. & Hardy, S. (1995). Reverse modelling of detachment folds; application to the Pico del Aguila anticline in the South Central Pyrenees (Spain). *Journal of Structural Geology* 17, 1707–1724.

Poblet, J., Muñoz, J.A., Travé, A & Serra-Kiel, J. (1998). Quantifying the kinematics of detachment folds using three-dimensional geometry: Application to the Mediano anticline (Pyrenees, Spain). *Geological Society of America Bulletin,* 110,111-125. DOI: 10.1130/0016-7606(1998)110<0111:QTKODF>2.3.CO;2

Puigdefàbregas, C. (1975). *La sedimentación molásica en la cuenca de Jaca*. Monografías del Instituto de Estudios Pirenaicos, 104. PhD thesis. Universitat de Barcelona. 188 pp.

Puigdefàbregas, C., Muñoz, J. A., & Verges, J. (1992). Trusting and foreland basin evolution in the southern Pyrenees. In: M. K. R. (ed.), *Thrust Tectonics*. Dordrecht: Springer. 247–254. DOI: 10.1007/978-94-011-3066-0_22

Puigdefàbregas, C. & Souquet, P. (1986). Tectosedimentary cycles and depositional sequences of the Mesozoic and Tertiary from the Pyrenees. Tectonophysics*,* 129, 173–203.

Remacha, E., Arbués, P., & Carreras, M. (1987). Precisiones sobre los limites de la secuencia deposicional de Jaca. Evolución de las facies desde la base de la secuencia hasta el techo de la arenisca de Sabiñánigo. *Boletin Geologico y Minero, 98,* 40-48.

Rodríguez-Pintó, A., Pueyo, E. L., Barnolas, A., Samsó, J. M., Pocoví, A., Gil-Peña, I., … Serra-Kiel, J. (2012a).

Lutetian magnetostratigraphy in the Santa Marina section (Balzes anticline, Southwestern Pyrenees). *Geo-Temas*, *13*, 1184–1187.

Rodríguez-Pintó, A., Pueyo, E. L., Serra-Kiel, J., Barnolas, A., Samsó, J. M., & Pocoví, A. (2013). The Upper Ypresian and Lutetian in San Pelegrín section (Southwestern Pyrenean Basin): Magnetostratigraphy and larger foraminifera correlation. *Palaeogeography, Palaeoclimatology, Palaeoecology, 370*, 13-29. DOI: 10.1016/j.palaeo.2012.10.029

Rodríguez-pintó, A., Pueyo, E. L., Serra-kiel, J., Samsó, J. M., Barnolas, A., & Pocoví, A. (2012b). Lutetian magnetostratigraphic calibration of larger foraminifera zonation (SBZ) in the Southern Pyrenees : The Isuela section. *Palaeogeography, Palaeoclimatology, Palaeoecology*, *333–334*, 107–120. DOI: 10.1016/j.palaeo.2012.03.012

Rodríguez-Pintó, A., Pueyo, E., Calvín, P., Sánchez, E., Ramajo, J., Casas, A., Ramón, M., & Pocoví, A. (2016). Rotational kinematics of a curved fold: The Balzes anticline (Southern Pyrenees). *Tectonophysics, 677–678,* 171–189. DOI: 10.1016/j.tecto.2016.02.049

Rodríguez-Salgado, P.; Falivene, O.; Frascati, A.; Arbués, P.; Monleon, O.; Butille, M.; Cabello, P.; Lopez-Blanco, M.; Poppelreiter, M.C. (accepted). Stratigraphic forward models of the Sobrarbe Deltaic Complex (Ainsa Basin, NE Spain): controls on stratigraphic architecture. In: Grotsch, J. (ed.), *EAGE Special Volume on Digital Geology.*

Roigé, M., Gómez-Gras, D., Remacha, E., Daza, R., & Boya, S. (2016). Tectonic control on sediment sources in the Jaca basin (Middle and Upper Eocene of the South-Central Pyrenees). *Comptes Rendus Geoscience*, *348*(3–4), 236–245. DOI: 10.1016/j.crte.2015.10.005

Romans, B. W., Castelltort, S., Covault, J. A., Fildani, A., & Walsh, J. P. (2016). Environmental signal propagation in sedimentary systems across timescales. *Earth-Science Reviews*, *153*, 7–29. DOI: 10.1016/j.earscirev.2015.07.012

Ross, W.C., Halliwell, B.A., May, J.A., Watts, D.E. & Syvitsky. (1994). Slope readjustment: A new model for the development of submarine fans and aprons. *Geology, 22*, 511-514.

Santolaria, P., Casas-Sainz, A.M., Soto, R. & Casas, A., (2016). Gravity modelling to assess salt tectonics in the western end of the South Pyrenean Central Unit. *Journal of the Geological Society*, *174,* 269–288. DOI: 10.1144/jgs2016-027

Sadler, P. M., & Jerolmack, D. J. (2014). Scaling laws for aggradation, denudation and progradation rates: the case for time-scale invariance at sediment sources and sinks. *Geological Society, London, Special Publications*, *404*, 69–88. DOI: 10.1144/SP404.7

Seguret, M. (1972). *Étude tectonique des nappes et séries décollées de la partie centrale du versant sud des Pyrénées – caractère synsédimentaire, rôle de la compression et de la gravité* (Série géol).

Montpellier: Publication de l'U.S.T.L.: Serie Géologie Structurale.

Silva-Casal, R., Aurell, M., Payros, A., Pueyo, E., Serra-Kiel, J. (2019). Carbonate ramp drowning caused by flexural subsidence: The South Pyrenean middle Eocene foreland basin. *Sedimentary Geology, 393-394*: 105538. DOI: 10.1016/j.sedgeo.2019.105538

Sinclair, H.D. (1997). Tectonostratigraphic model for underfilled peripheral foreland basins: an Alpine perspective. *Geological Society of America Bulletin, 109*, 324-346.

Soler-Sampere, M., & Puigdefàbregas, C. (1970). Líneas generales de la geología del Alto Aragón Occidental. *Pirineos*, *96*, 5–19.

Soto, R., & Casas, A. M. (2001). Geometría y cinemática de las estructuras Norte-Sur de la Cuenca de Aínsa. *Revista de La Sociedad Geológica de España*, *14*(3–4), 199–211.

Soto, R., Casas, A. M., Sorti, F. & Faccenna, C. (2002). Role of lateral thickness variations on the development of oblique structures at the western end of the South Pyrenean Central Unit. *Tectonophysics*, *350*, 215–235.

van Lunsen, H. A. (1970). *Geology of the Ara-Cinca region, Spanish Pyrenees, Province of Huesca*. Utrecht State University.

Vincent, S. (2001) The Sis palaeovalley: a record of proximal fuvial sedimentation and drainage basin development in response to Pyrenean mountain building. *Sedimentology*, *48*, 1235-1276.

Walsh, J.P., Nittrouer, C.A., Palinkas, C.M., Ogston, A.S., Sternberg, R.W. & Brunskill, G.J. (2004). Clinoform mechanics in the Gulf of Papua, New Guinea. *Continental Shelf Research, 24,* 2487–2510.

Wuellner, D.E.Lehtonen, L.R., James, W.C. (1986). Sedimentary-tectonic development of the Marathon and Val Verde basins, West Texas, USA: a Permo-Carboniferous migrating foredeep. In: Allen P.A., Homewood, P. (Eds.) *Foreland Basins.* IAS Special Publication 8. 347-368.

Zoetemeijer, R., Desegaulx, P., Cloetingh, S., Roure, F., & Moretti, I. (1990). Lithospheric Dynamics and Tectonic-Stratigraphic Evolution of the Ebro Basin. *Journal of Geophysical Research*, *95* (B3), 2701–2711. DOI: 10.1029/JB095iB03p02701

Table captions:

Table 1: Relation of published magnetostratigraphic sections and the exclusion criteria marked with "X": (1) Average number of samples/magnetozones lower than 8. (2) Large number of magnetic reversals on the GPTS not found on the magnetostratigraphic log. (3) Data far-off from the studied profile. (4) Not the best log at a specific location, with respect to the overall quality of the data. The sections selected for this study are indicated in bold, see their location in Figure 2.

Table 2: Mean paleomagnetic directions and corresponding fisher statistics of the Olsón and Yebra de Basa sections.

Table 3: SR for the studied logs including decompacted SR for each significant magnetozone and average original (compacted) and decompacted SR for each log or successive pair of logs.

Figure captions

Figure 1: Evolution of a Foreland basin system controlled by a piggy-back foreland-directed thrust sequence with the location of Proximal and Distal Foreland Basin Systems, Wedge-top, Foredeep, Forebulge and Backbulge depozones. (a) Initial stage with a foredeep depozone located on the footwall of the active thrust. (b) A second thrust produces a displacement of the subsidence towards the foreland and migration of the forebulge. The original forebulge (FB1) is now buried below the second foredeep depozone associated with the second thrust. (c) Initial movement of a third thrust produces a forelandward displacement of subsidence and migration of the forebulge. Original forebulge (FB1) is now incorporated into the hanging wall of the thrust, while the foredeep sediments associated with the second thrust (FB2) are buried below the wedge-top depozone (piggy-back basin) sediments. (d) Final movement of a third thrust produces foreland displacement of subsidence and migration of the forebulge. Original forebulge (FB1), incorporated into the hanging wall of the thrust suffers from denudation as it becomes part of the uplifted source area. (e) Ideal log showing the vertical superposition of depozones as deformation advances to the foreland as well as sedimentary and accommodation trends. See its representative location in frame (c).

Figure 2: Geological setting of the South-central Pyrenees. (a) Geological maps with the location of the main structures, basins, the position of the cross-sections in Figure 2b, studied logs and Figure 7 profiles. Thrust Sheets: CB: Cotiella-Boixols; PM: Peña Montañesa-Montsec; EM: Sierras Exteriores-Serres Marginals. Thrust: Ot: Oturia thrust. Folds: 1: Balzes; 2: Boltaña; 3: Buil 4: Mediano. Sections: GA: Río Gállego-Río Aragón; YB: Yebra de Basa; IS: Isuela; BL: Belsué; SM: Santa Marina; CM: Coscollar-Mondot; MD: Mediano; OL: Olsón; ES: Ésera; LS: Lascuarre; PS: Pobla de Segur. The new sampled logs (Olsón and Yebra de Basa) are marked in red. This map was modified from the compilation made by Fernández-Bellón (2004) from published 1:50,000, 1:100,000 and 1:200,000 scale maps, and unpublished mapping by researchers from the Universitat de Barcelona. (b) Cross-sections from the study area showing the structural arrangement in four different transects. Middle Eocene sediments have been distinguished to easily outline the studied strata. Approximate projected position of the studied logs is included. Modified from Berástegui *et al.*, 1993 (B1); Muñoz *et al.*, 2013 (B2); and Labaume & Teixell, 2018 (B3 and B4).

Figure 3: Stratigraphic diagram of the Tremp-Graus-Ainsa-Jaca basin, with the different stratigraphic units, approximate location of studied logs and sedimentary environments.

Figure 4: Olsón (Ainsa Basin) and Yebra de Basa (Jaca Basin) magnetostratigraphic logs. Black dots represent high quality paleomagnetic directions and white dots represent intermediate quality. Triangles represent low quality paleomagnetic directions. In the Olsón log, VGPs are corrected for a 30° clockwise rotation.

Figure 5: ChRM calculated from 72.8% of the total of the samples processed in the laboratory. The resulting mean direction of the Olsón log records a 30° clockwise rotation and the mean direction of the Yebra de Basa log does not yield any significant vertical-axis rotation.

Figure 6: Magnetostratigraphic correlation of the new logs with the GPTS (Gradstein *et al.*, 2012), helped by the stratigraphic correlation with the Río Gállego/Río Aragón log (Oms *et al.*, 2003) and with the Coscollar-Mondot logs (Mochales *et al.*, 2012).

Figure 7: Correlation among the Tremp, Ainsa, and Jaca sub-basins through the N-Profile and the S-Profile showing: (a) the main depositional environments, and (b) the lateral and vertical SR variations through the studied logs. Location of the profiles and logs is shown in Figure 2.

Figure 8: Compacted and decompacted SR diagrams for each of the studied logs in this work, including references to the stratigraphic units and formations. The vertical axis is stratigraphic height in meters and the horizontal axis is the age, in Ma. Segments are colored according to their SR following the color legend in Figure 7.

Figure 9: Evolution of decompacted SR across the Tremp-Jaca basin over time following the N-Profile and the S-Profile. 16 Graphs show SR variation for each time-slice (magnetostratigraphic chron) and distribution of the main facies belts. Vertical scale: SR in cm/kyr; horizontal scale: distance in km. Absolute ages from GPTS (Gradstein *et al.*, 2012). Individual SR for each log are indicated. Background colors represent the attribution of the logs to the different depozones. The logs used are: BL, Belsué; IS, Isuela; SM, Santa Marina; GA, Gállego-Aragón; YB, Yebra de Basa; OL, Olsón; CM, Coscollar-Mondot; MD, Mediano; ES, Ésera; LS, Lascuarre; PS, Pobla de Segur. Dashed logs and SR curves indicate minimum values due to incomplete logs. Duration of each magnetozone is indicated in Myr. The SR graphs have been produced from the data obtained on the studied logs. Only variations related to Boltaña and Balzes anticline growth have been inferred since these structures have an important role on SR evolution and distribution.

Figure 10: Map view evolution of SR across the TJB over time. Each time step corresponds to a different chron as shown in Figure 9. Coordinates are in km in the UTM reference system. This map shows the present-day location of structures and logs and the trace of Figure 9 profiles through the logs considered for each chron. Absolute ages from GPTS (Gradstein *et al.*, 2012). The shortening related to thrust advance and clockwise synsedimentary rotation of the Ainsa Basin and External sierras structures has not been taken into account (Palinspastic reconstruction is not considered). The Montsec-Peña Montañesa thrust has been used as a reference since it was not an active structure during the studied interval. Paleocurrent data from Arbués *et al.* (2011); Puigdefàbregas (1975); Michael *et al.* (2014); Roigé *et al.* (2016); Barsó (2007); Vincent (2001), and our own data. J: Jaca, A: Ainsa, G: Graus, T: Tremp. SR variations

related to anticline growth have not been inferred except Boltaña and Balzes folds due to their influence on clastic sediment routing. Cotefablo, Banastón and Jaca are turbidite systems of the Hecho group in the Jaca basin (Mutti *et al.*, 1985; Labaume *et al.*, 1987). Morillo, Coscojuela, Gabardilla, O Grao and Guaso are turbidite systems in the San Vicente Formation in the northern Ainsa Basin (Arbués *et al.*, 2011; Muñoz *et al.*, 2013). Sobrarbe 1: Deltaics older than San Lino horizon (Arbués *et al.*, 2011) in Ainsa; Sobrarbe 2: Sobrarbe Deltaic Complex below Buil nummulite banks; Sobrarbe 3: Sobrarbe Deltaic Complex above Buil nummulite banks.

Figure 11: Evolution of a foreland basin system where a foredeep with underfilled accommodation is later incorporated into a wedge-top depozone in a thrust-flat position without major uplift. This evolution results in an early wedge-top stage having high SR and relatively low SR in the area where the proximal Foredeep should be developed. Vertical scale exaggerated. (a) Initial underfilled foredeep situation. (b) Wedge-top situation keeping higher SR than other depozones.

Figure 12: General conceptual models showing the geometry of shelf margins parallel to the main sediment transport direction from non-marine to deep sea areas showing the location of the sedimentary depocenters in different situations: a) Normal regression in a graded prograding clastic shelf; b) Evolution of two successive regressive episodes where the advance of the graded clastic shelf produces a retreat of the carbonate facies; c) Accretionary transgression; d) Normal regression with steepening of the shelf margin and tectonically induced subsidence preventing the overfilling of the accommodation of the sedimentary trough. This last case shows the alternating deposition of deep marine turbidites during out-of-grade episodes and the progradation of clastic graded shelfs in more stable periods.

Figure 13: Mutual influence and feedback among tectonics, sedimentation, and salt migration as a hypothesis to explain the abnormal SR in the Escanilla Formation in the Ainsa Basin during the uppermost Lutetian and lowermost Bartonian. (a) Flow diagram. (b), (c), and (d) simplified not-to-scale E-W evolutive sections from C20n (b) to c19n (d).

Magnetostratigraphic section	*Reference*	*1*	*2*	*3*	*4*
Pobla de Segur (PS)	Beamud *et al.*, 2003				
Sis	Beamud *et al.*, 2003				X
Roda	Bentham & Burbank, 1996	X			
Esplans	Bentham & Burbank, 1996	X			
Lascuarre (LS)	Bentham, 1992				
Esera (ES)	Bentham, 1992				
Mediano (MD)	Bentham, 1992				
Eripol	Bentham, 1992	X	X		
Almazorre	Bentham, 1992	X			X
Liguerre	Bentham, 1992		X		
Belsué (BL)	Garcés *et al.*, 2014				
Salinas	Hogan & Burbank, 1996			X	
Arguís/Monrepós	Hogan & Burbank, 1996				X
Yebra de Basa	Hogan & Burbank, 1996		X		
San Felices	Hogan & Burbank, 1996				X
Agüero	Hogan & Burbank, 1996				X
Ayerbe	Hogan & Burbank, 1996				X
Arguís/Pico del Águila	Kodama *et al.*, 2010				X
Mondot (CM)	Mochales *et al.*, 2012				
Coscollar (CM)	Mochales *et al.*, 2012				
Río Gállego/Río Aragón (GA)	Oms *et al.*, 2003				
Santa Marina (SM)	Rodríguez-Pintó *et al.*, 2012 (a)				
Isuela (IS)	Rodríguez-Pintó *et al.*, 2012 (b)				
San Pelegrín	Rodríguez-Pintó *et al.*, 2013				X

Section	*N*	*dec*	*inc*	α_{95}	*k*
Olsón					
Normal	90	029.0	43.2	5.8	8
Reversed	46	207.2	-22.6	12.8	4
all to normal	136	028.6	38.3	4.2	6
Yebra de Basa					
Normal	146	009.7	42.4	3.7	11
Reversed	29	193.8	-42.6	14.6	4

Area	Sect.	Magnetozone	duration (Myr)	Original thickness (m)	decompacted thickness (m)	decompact. SR (cm/kyr)	orig. mean SR (cm/kyr)		decom. mean SR (cm/kyr)	
Southern Jaca basin	Belsué	Overburden	-	2200	-	-	15.39	11.04	23.06	17.17
		C16n	0.994	>189.00	>293.83	>29.56				
		C16r	0.269	98.50	150.21	55.84				
		C17n1n	0.816	67.90	93.49	11.46				
		C17n3 + C17n1r	0.595	138.60	205.00	34.45				
		C17r	0.288	46.00	65.19	22.64				
		C18n.1n	1.018	156.80	215.75	21.19				
		C18n2n+C18n1r	0.515	106.30	186.06	36.13				
		C18r	1	78.90	122.95	9.94				
	Isuela	Overburden	-	3100	-	-	6.45		11.49	
		C19n	0.234	>49.59	>97.85	>41.82				
		C19r	0.913	128.5	226.66	24.83				
		C20n	1.154	156.38	278.32	24.12				
		C20r	2.437	88.75	163.01	6.69				
		C21n	1.895	39.42	67.42	3.56				
		C21r	1.265	>27.72	>51.05	>4.04				
	Santa Marina	Overburden	-	3000	-	-	8.99		15.88	
		C19n	0.234	29.11	54.14	23.14				
		C19r	0.913	278.86	458.14	50.18				
		C20n	1.154	105.02	195.80	16.97				
		C20r	2.437	153.82	288.69	11.85				
		C21n	1.895	29.41	56.40	2.98				
		C21r	1.265	>29.78	>60.41	>4.78				
Ainsa basin	Coscollar - Mondot	Overburden	-	970	-	-	14.57	16.27	20.67	21.53
		C18r	1.003	>80.00	>104.17	>10.39				
		C19n	0.234	71.00	93.57	39.99				
		C19r	0.913	314.00	411.34	45.05				
		C20n	1.154	359.00	500.36	43.36				
		C20r	2.437	284.00	425.94	17.48				
		C21n	1.895	44.00	72.47	3.82				
		C21r	1.265	79.00	129.11	10.21				
	Olsón	Overburden	-	300	-	-	20.36		23.59	
		C17n2r + C17n1r	0.277	31.50	34.63	15.26				
		C17n3n	0.178	50.00	55.68	31.28				
		C17r	0.288	53.00	61.30	21.29				
		C18n	1.533	296.80	332.26	21.67				
		C18r	1.003	236.20	289.76	28.89				
	Mediano	Overburden	-	470	-	-	19.03	23.37	25.20	30.09
		C18n	1.533	>104.71	>120.37	>7.85				
		C18r	1.003	247.17	285.51	28.47				
		C19n	0.234	96.39	119.57	51.10				
		C19r	0.913	171.73	216.01	23.66				
		C20n	1.154	600.45	786.98	68.20				
		C20r	2.437	337.76	516.31	21.19				
		C21n	1.895	>135.10	>224.50	>11.85				

Area	Sect.	Magnetozone	duration (Myr)	Original thickness (m)	decompacted thickness (m)	decompact. SR (cm/kyr)	orig. mean SR (cm/kyr)		decom. mean SR (cm/kyr)	
Tremp-Graus basin	Esera	Overburden	-	600	-	-	21.00		25.62	
		C20r	2.437	>469.87	>557.82	>22.89				
		C21n	1.895	>439.72	>552.03	>29.31				
	Lascuarre	Overburden	-	300	-	-	8.67		9.83	
		C17r	0.288	29.65	31.51	10.94				
		C18n	1.533	89.73	96.84	6.32				
		C18r	1.003	105.78	122.63	12.23				
		C19n	0.234	39.89	49.47	21.14				
	Pobla de Segur	Overburden	-	210	-	-	8.27		8.93	
		C15n	0.295	41.65	43.34	14.69				
		C18n + C15r	4.907	205.23	214.60	4.37				
		C19n + C18r	1.237	285.83	317.37	9.61				
Northern Jaca basin	Yebra de Basa	Overburden	-	1200	-	-	48.95	53.25	72.49	84.54
		C17n	1.411	322.00	432.65	30.66				
		C17r	0.288	100.00	153.86	53.42				
		C18n.1n	1.018	708.00	1003.04	98.53				
		C18n.1r	0.07	61.00	118.86	169.80				
		C18n.2n	0.445	391.00	634.45	142.57				
		C18r	1.003	>53	>107.43	>10.71				
	Río Gallego - Río Aragón	Overburden	-	2800	-	-	57.46		96.33	
		C18r	1.003	637.12	1058.07	105.49				
		C19n	0.234	57.83	123.53	52.79				
		C19r	0.913	557.85	920.26	100.80				
		C20n	1.154	645.56	1080.84	93.66				
		C20r	2.437	>256.54	>456.05	>18.71				

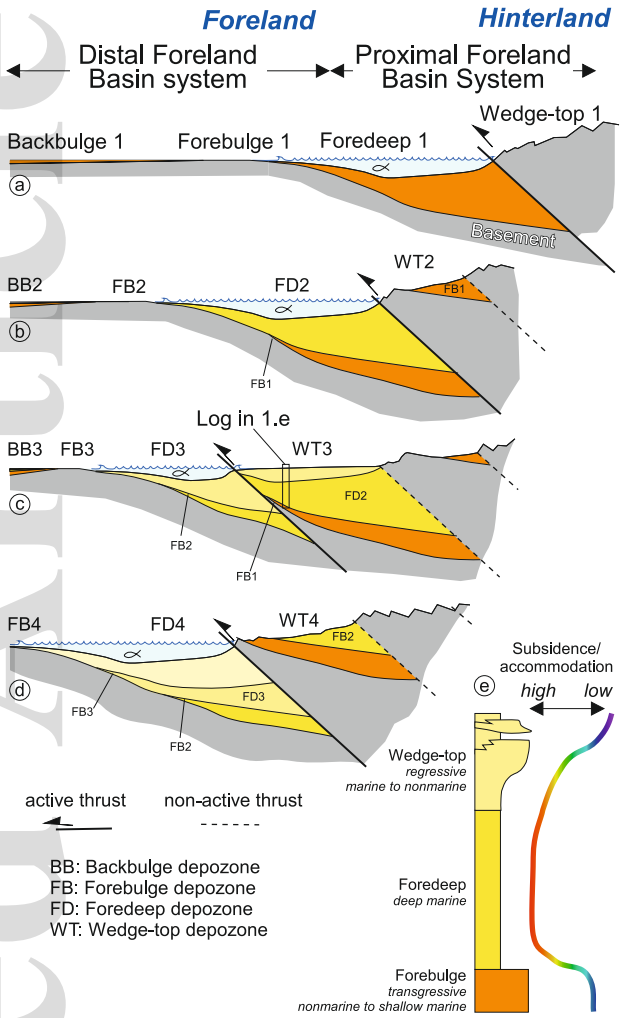

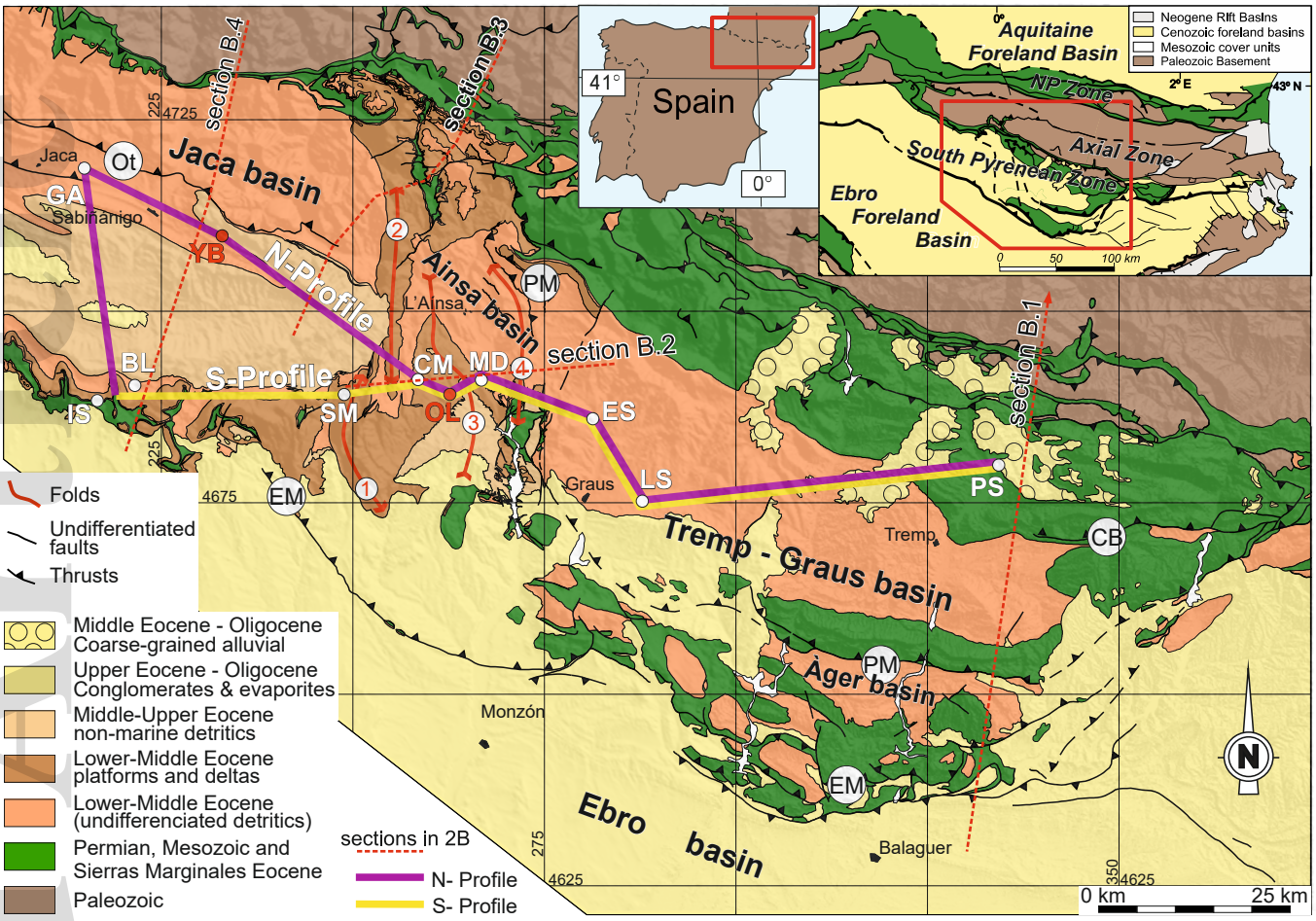

Figure 2A

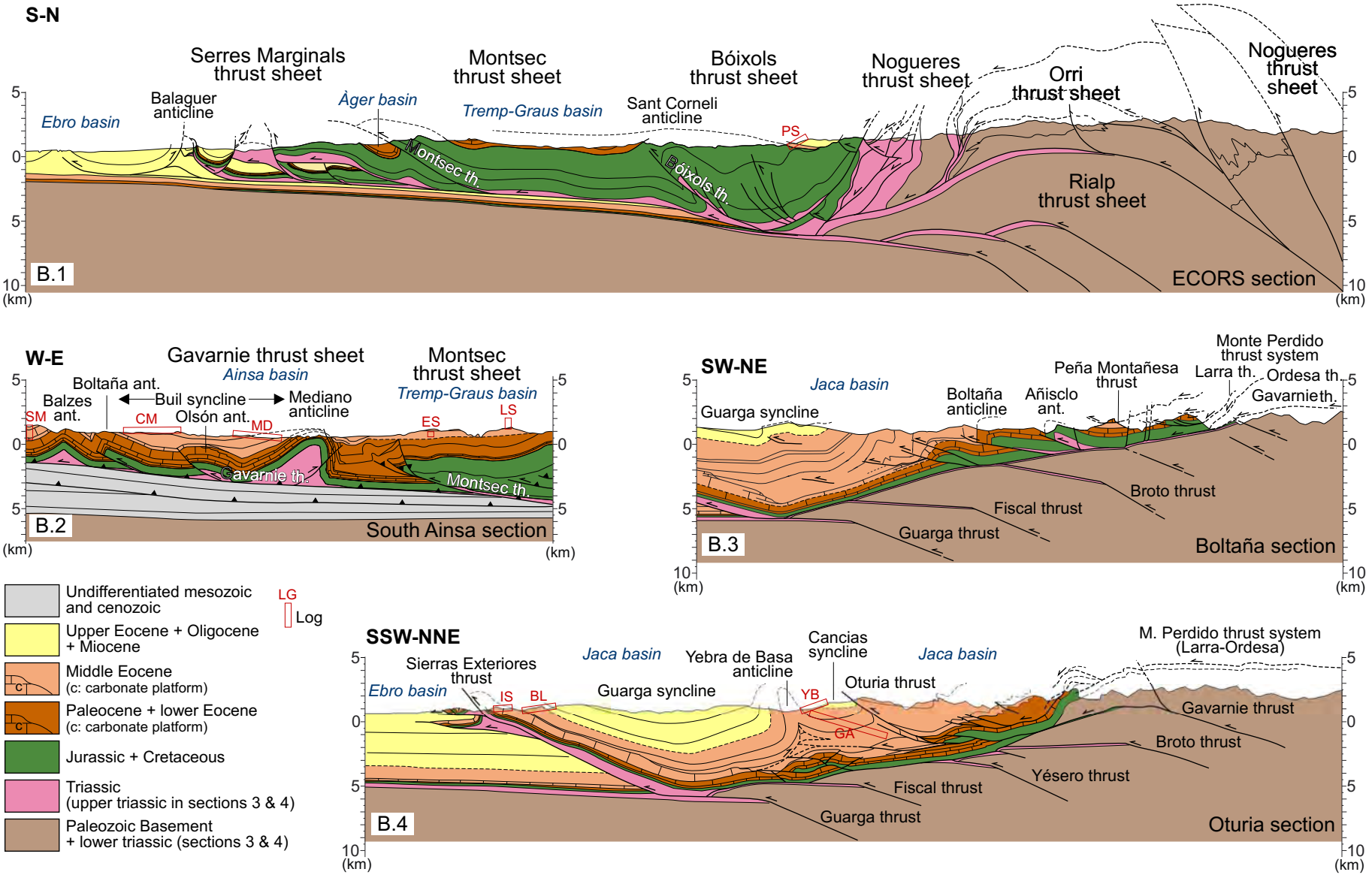

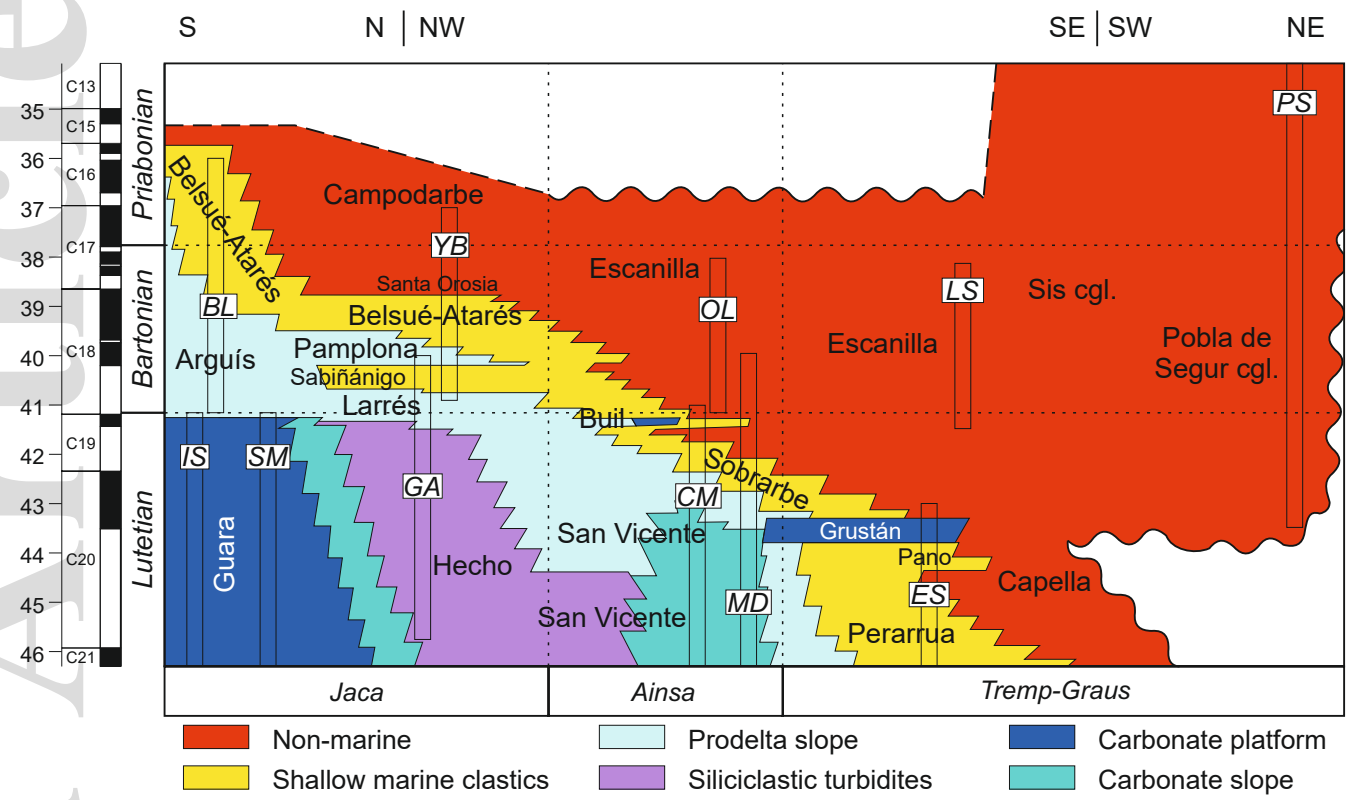

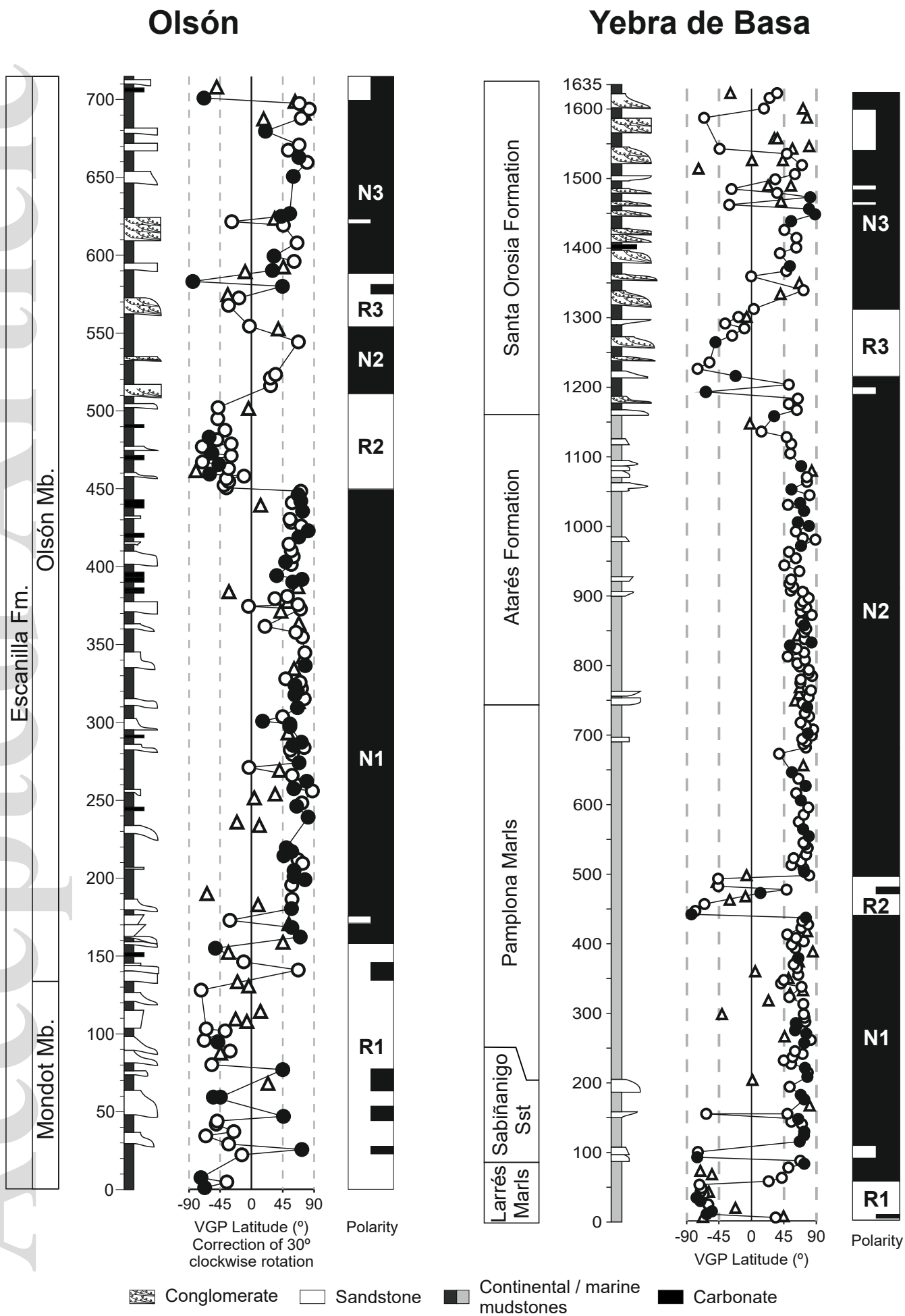

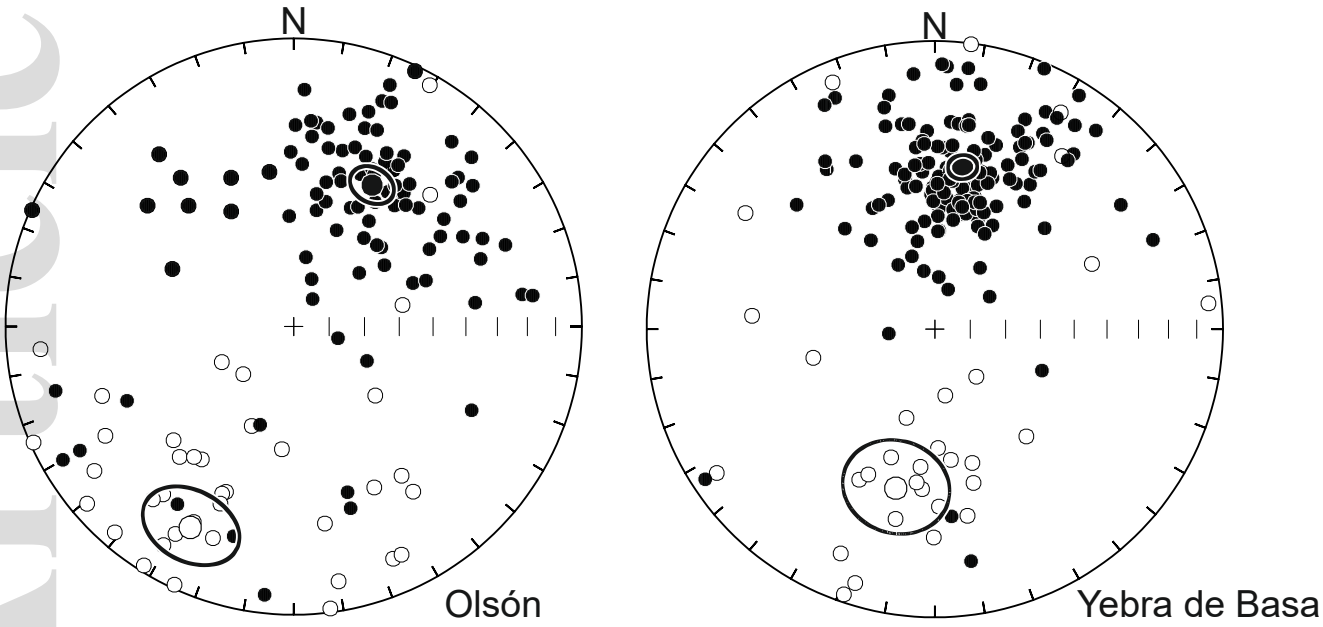

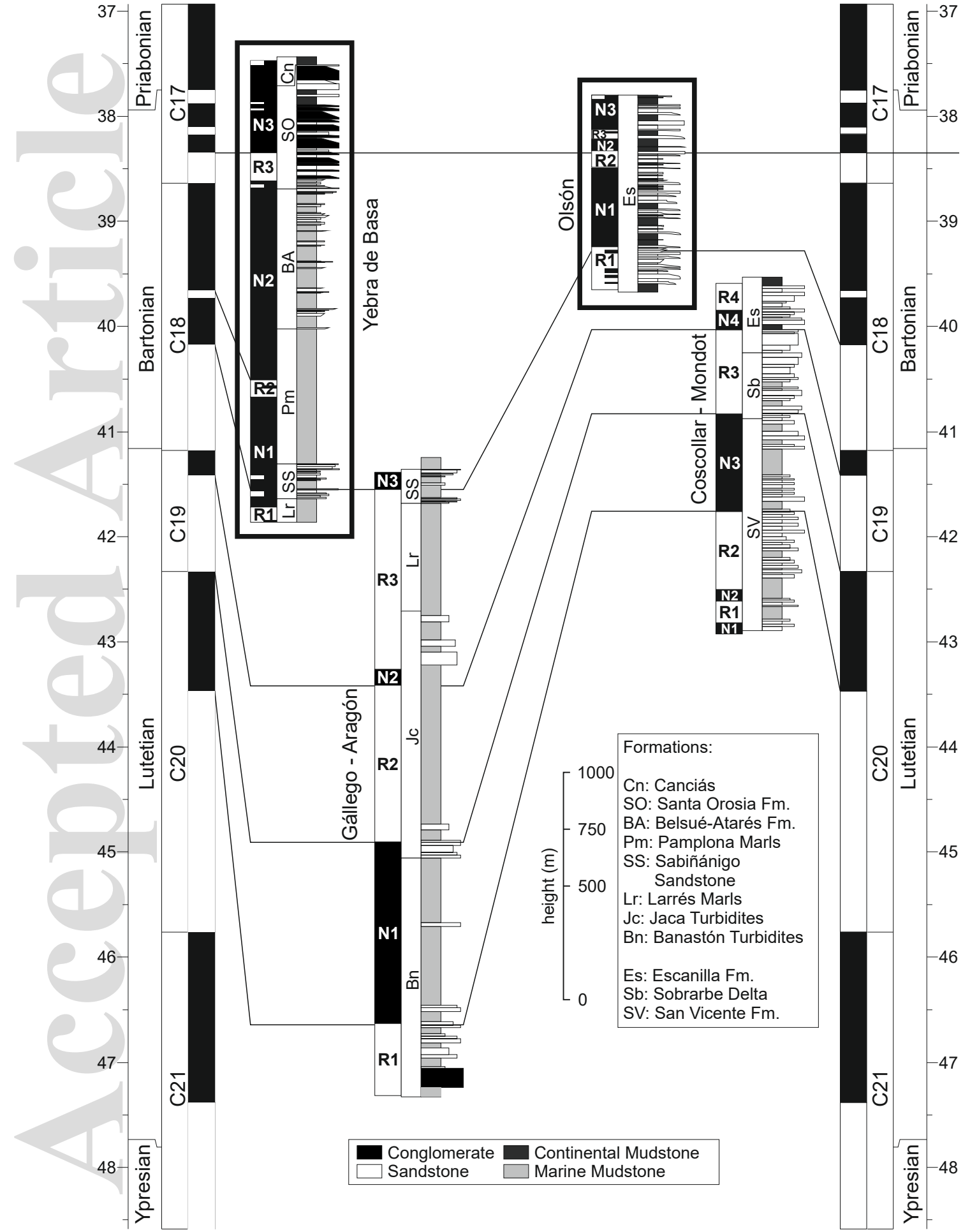

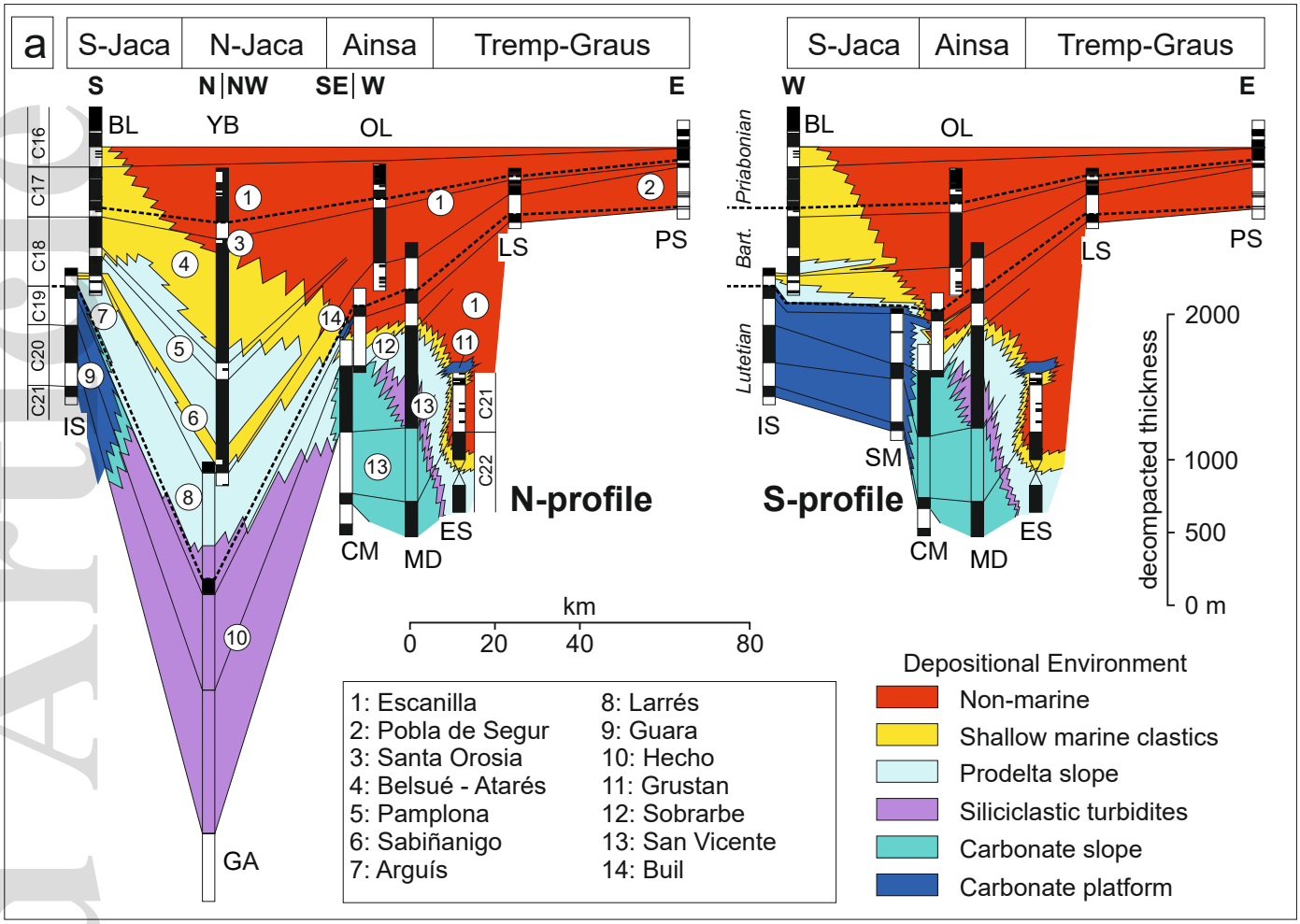

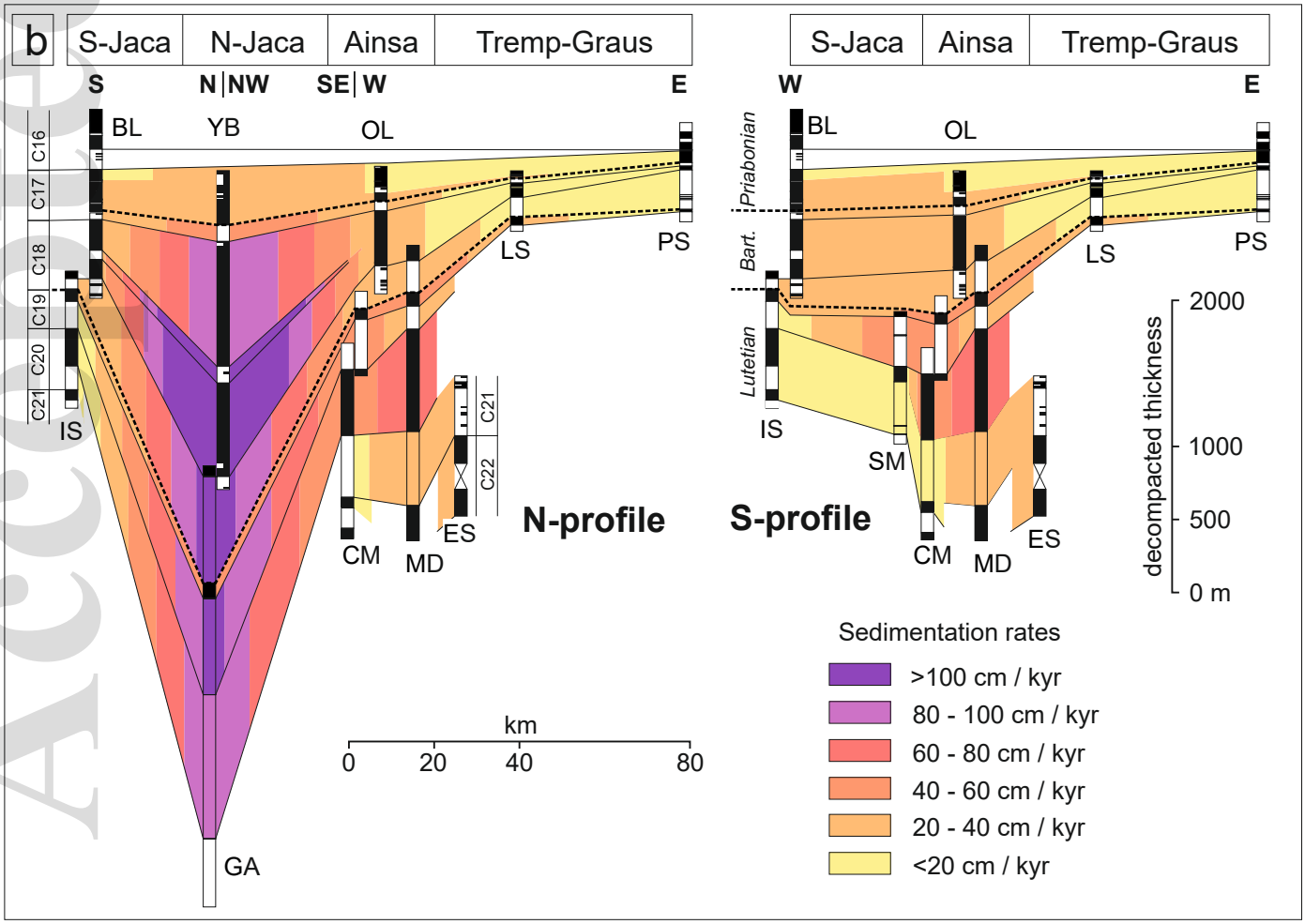

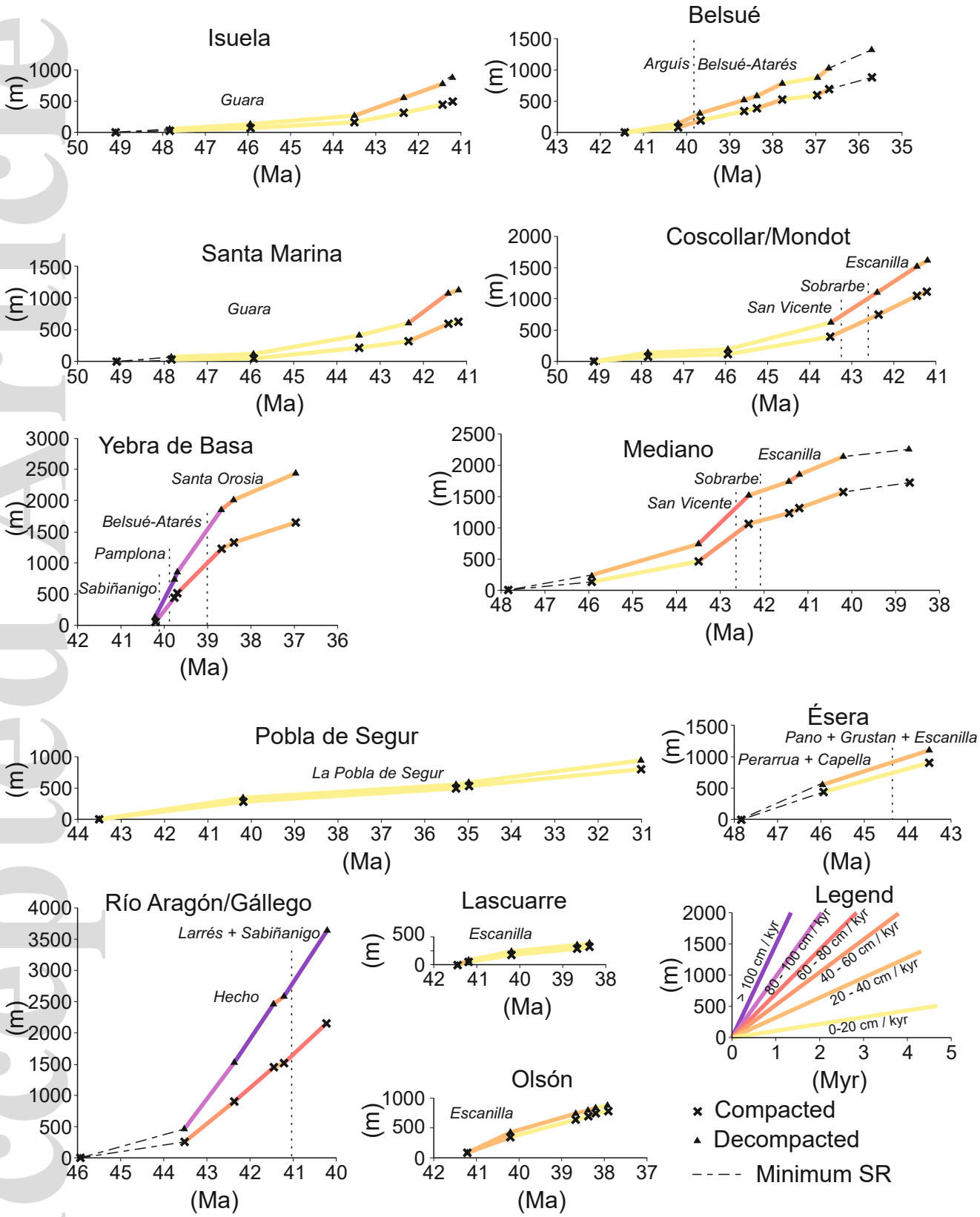

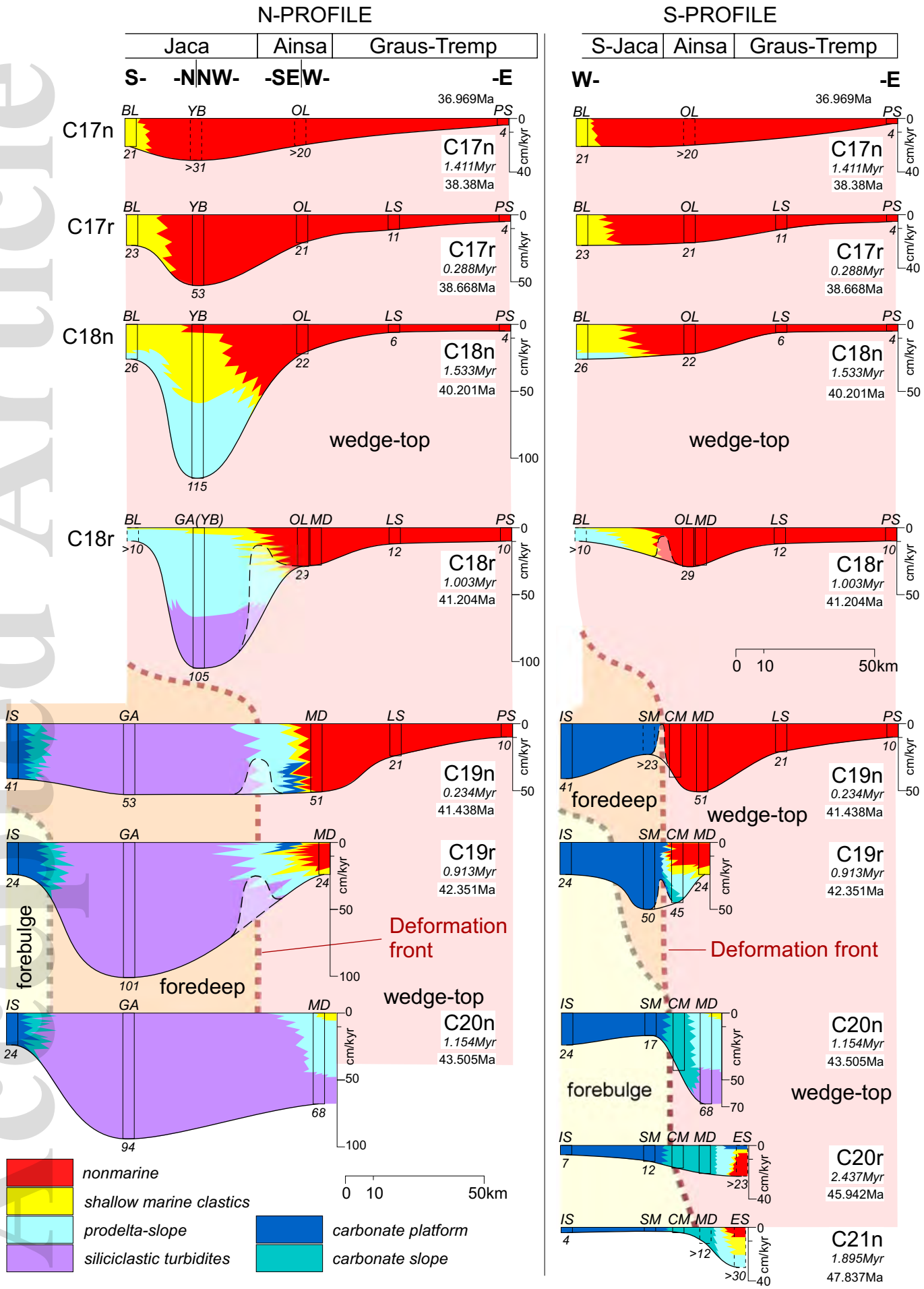

Figure 9

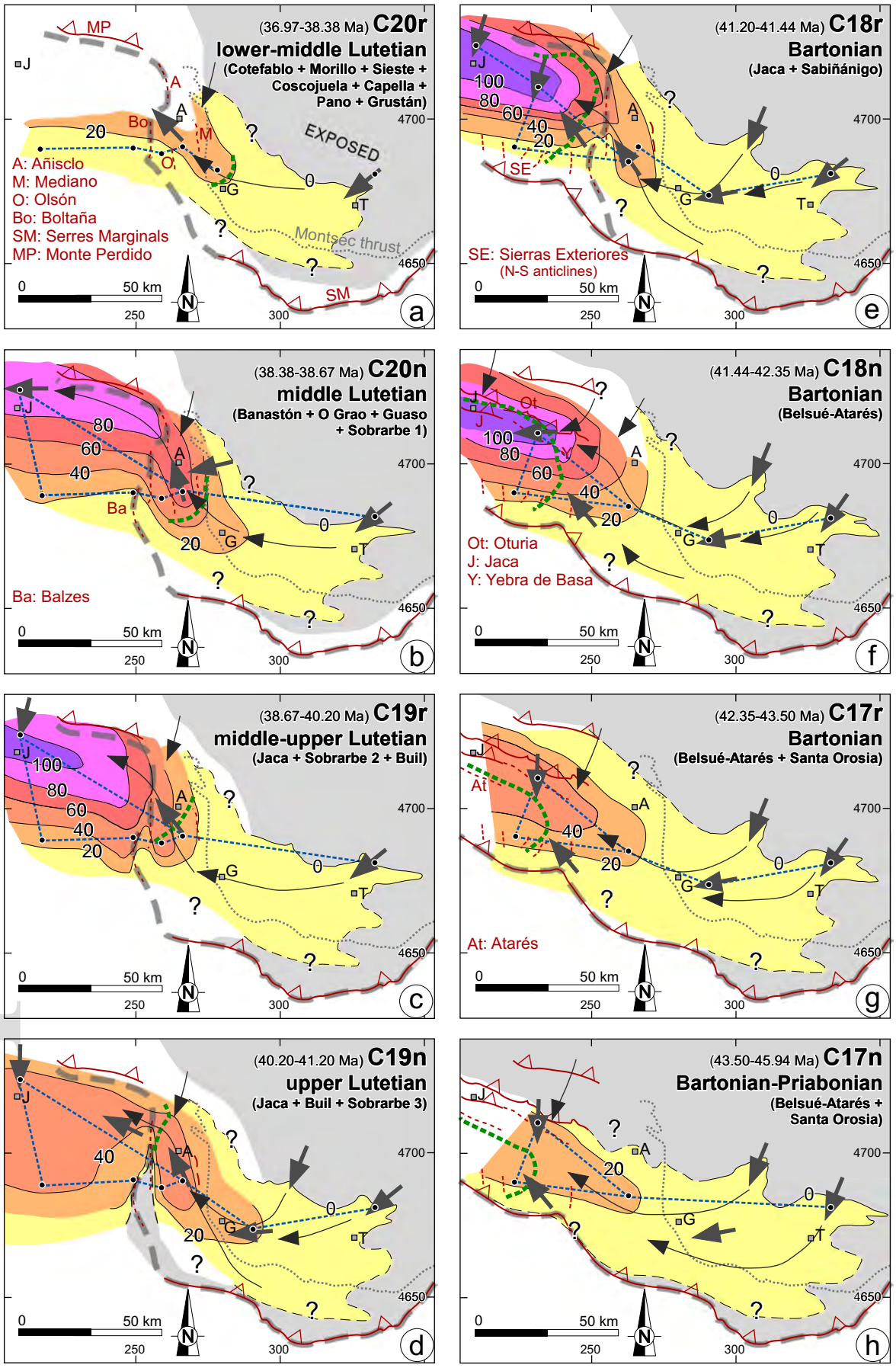

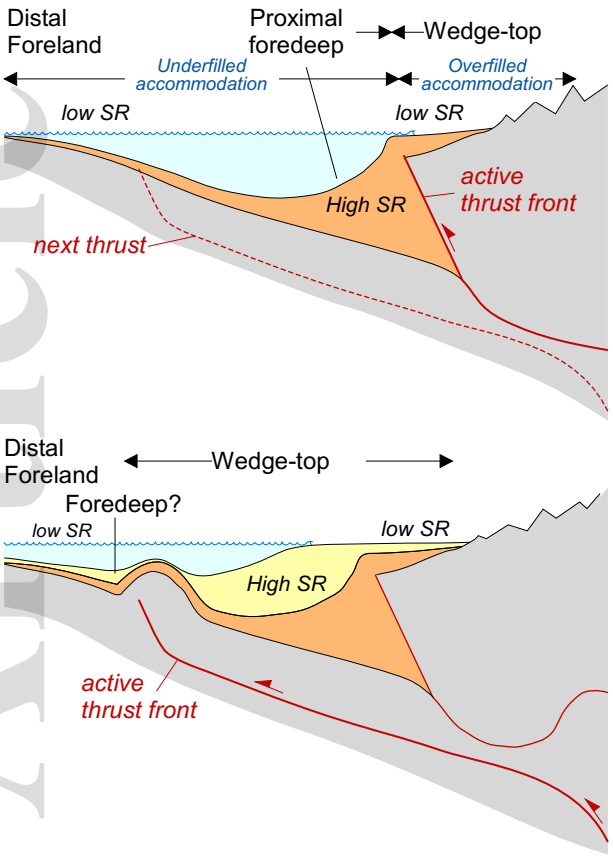

Figure 11

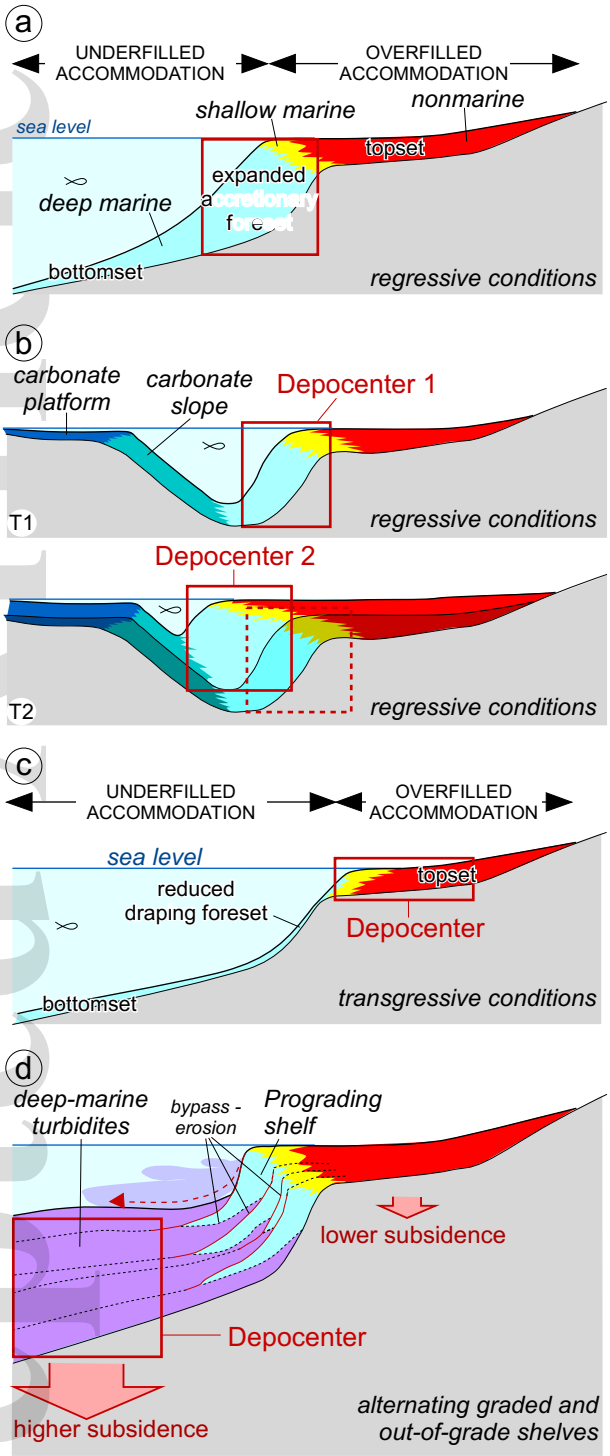

Figure 12

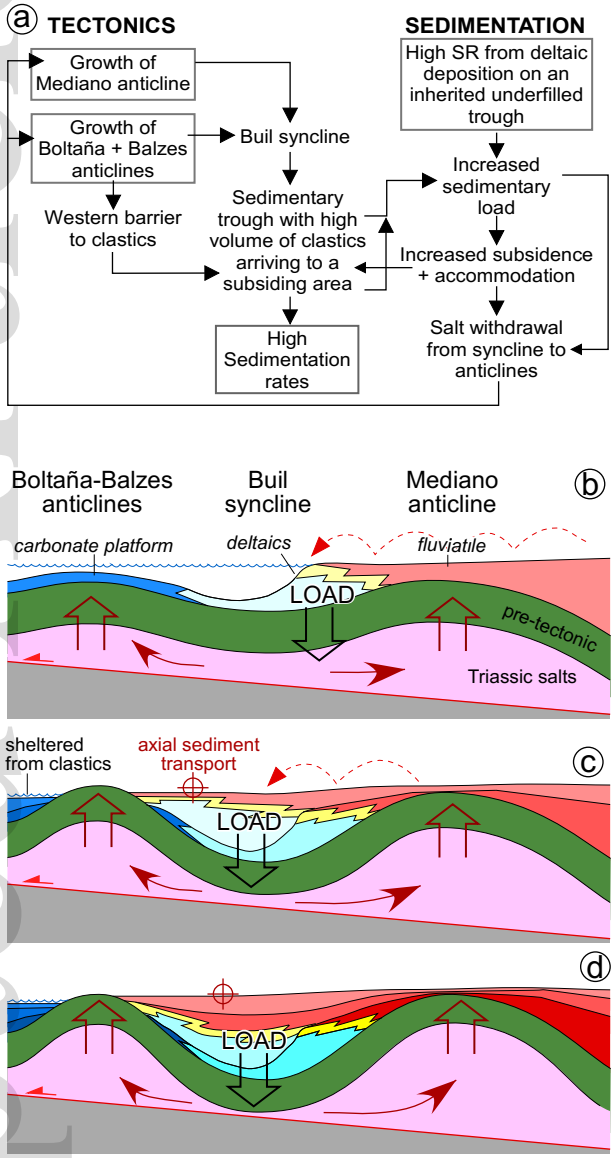

Figure 13